Labrador Sea winter heat and freshwater content observations from glider and Argo data

Nicolai von Oppeln-Bronikowski[1], Brad de Young[1], Eleanor Frajka-Williams[2], Ilona Goszczko[3]and Louis Clément[2]

[1]Memorial University, Department of Physics and Physical Oceanography, St. John's, NL, Canada
[2]National Oceanography Centre, Southampton,United Kingdom
[3]Institute of Oceanology, PAN, Sopot, Poland

Key Points:

- We use a glider survey and Argo profiles in the Central Labrador Sea during the winter season 2020 to estimate mixed layer depths, heat and freshwater content and the role of eddies.
- We find that overall convection during the 2019-2020 winter is weakened compared to previous years, but that despite this trend individual Argo profile that convection reached to almost 2000 m .
- From the glider data we calculate correlation scales and find that scales, possibly also due to the eddies, exhibit strong heterogeneity rendering local small-scale processes important.
- We explore the discrepancy between Argo and the glider observations in terms of the impact on the Labrador Sea freshwater budget, suggesting that the glider data offers useful information not captured by the existing Argo float observations.

Corresponding author: Nicolai von Oppeln-Bronikowski, nbronikowski@mun.ca

Abstract

The Labrador Sea undergoes deep mixing in the wintertime, with mixed layer depths frequently reaching down to 2000 m. The resulting water mass that is formed - Labrador Sea Water (LSW) - has long been thought to be important for the deep Western Boundary Current (dWBC) and the upper limb of the AMOC. Direct observations of the overturning have, however, been rather limited. Limited Argo profiles and moorings in key locations offered winter measurements in a region challenged by severe weather conditions. Here we discuss observations of a winter-spring glider deployment in the Labrador Sea, but more specifically where deep convection occurs, from December 2019- to June 2020. Using the glider data, we describe the evolution of the mixed layer, changes in heat and freshwater content for surface (0-500 m) and intermediate depth (500-1000 m) layers for the central Labrador Sea convection region inside a box 200 by 100 km wide and spatial scales of T and S. We compare the observations with reanalysis data (air-sea heat fluxes and winds) and Argo profiles to better understand the variability missed by existing datasets. These observations highlight the role played by eddies in the overall variability of heat and salt in this region, something that is missed by Argo observations. They also show changes in spatial scales of T-S over the months from January to May, pointing towards the modulating effect of eddies on LSW winter formation.

Plain Language Summary

In this paper we describe the Labrador Sea winter-time convection period based on observations from an ocean glider and Argo floats. The data reveal that mixed layer depths reached nearly 2000 m in the winter of 2020. There is good agreement between the Argo and glider data, although the glider resolves spatial-temporal dynamics not captured by Argo. Such variability is important to resolve the amount of freshwater in the Labrador Sea. Freshwater content is important for different reasons, one of which is its role in constraining convection. Because the Labrador Sea is a key place to understanding the global overturning circulation, our study suggests that glider data provide useful information not captured by existing Argo float observations.

1 Introduction

The Labrador Sea plays an outsized role in influencing the large-scale climate circulation as one of the few regions where water convects to depths of 2000 m. Winter convection driven by strong winds and storms drives oceanic mixing frequently exceeding depths of 1000 m and large water mass formation of Labrador Sea Water (LSW). Through subduction and outflow within the the deep-Western Boundary Current (dWBC), LSW is present in much of the North Atlantic and beyond. Historically, convection in the Labrador Sea was thought to serve as the downwelling limb of the Atlantic meridional overturning circulation (AMOC), and that its intensity would be related to the strength of the overturning (Clarke & Gascard, 1983; Aagaard & Carmack, 1989). However, OSNAP measurements (Lozier et al., 2019; Li et al., 2021) appear to show only a minor role for Labrador Sea convection, and comparisons between overturning transport at 45N and air-sea transformation to the north of 45N (Desbruyères et al., 2019) suggest that the reason convection and LSW formation do not imprint on transports is because the waters entering the Labrador Sea - prior to convection - are already denser than the waters of density of maximum overturning. While the relationship between deep water formation and the MOC remains uncertain, it is clear that the ventilation that occurs in regions of deep water formation plays a role of hotspots for the storage of anthropogenic carbon (Khatiwala et al., 2013) and the supply of oxygen to the deep ocean (Körtzinger et al., 2008; Koelling et al., 2017).

The large scale processes connected to deep convection and formation of LSW have been described in various studies (Clarke & Gascard, 1983; Lilly et al., 1999; Yashayaev

& Loder, 2016). These studies are in general agreement over the location and mechanisms behind LSW water formation in the months from February to April when heat loss reaches its maximum. These studies in also point to significant variability on annual and decadal scales in the properties and volume of LSW. It is also accepted that significant water property (T-S, gasses, nutrients) modification occurs at sub-mesoscale length scales (Tagklis et al., 2020). Winter storms on 5–10 day timescales (Sathiyamoorthy & Moore, 2002) can trigger heat loss exceeding 1500 W m^{-2}. Boundary currents generate fresh and salty eddies shedding in regions of steep topography (Lilly et al., 2003; Lilly & Rhines, 2002). These eddies can be sources of salt or heat that can alter stratification and either add or remove buoyancy, decreasing or enhancing convection. Not all eddies form at the shelf break with some formed as a result of local instability during convective mixing. These still could be responsible for significant contribution to winter heat loss (Gelderloos et al., 2011). Beyond the smaller scale features, the oceanographic conditions in the Labrador Sea change on annual and multi-annual time-scales, with convection intensifying in certain phases and weakening in others (Clarke & Gascard, 1983; Gascard & Clarke, 1983; Yashayaev, 2007; Yashayaev & Loder, 2016). The important role and influence of this ocean region supports and ongoing observing presence.

The Labrador Sea is well-known for its extreme winter weather and sea states – with significant wave heights regularly exceeding 10 m, winter winds stronger than 30 m s^{-1} and atmospheric temperatures below -20 °C (Renfrew & Moore, 1999; Moore et al., 2008). These conditions pose challenges for any observational programs. Prior to the Argo program, most of the data for the Labrador Sea came from moorings and hydrographic ship cruises. These programs, in particular the WOCE, provided seasonally-biased (towards non-winter seasons) snapshots or point-measurement time series (BRAVO) but it was not until the Argo program that a more holistic view of the Labrador Sea emerged. The presence of floats in all of the Atlantic, allowed exploration of the larger-scale picture of LSW spreading (Fischer et al., 2018), however, Argo does not close all gaps in tracking LSW. For one, Argo is designed to capture seasonal variability at a 3° by 3° spatial scale, and to this end, each float spends approximately 10 days at 1000 m between profiles. These scales are much larger than eddies that are thought to be important for the heat exchange (Hátún et al., 2007) and larger than the winter mixing plumes at these latitudes (Mertens, 2000). Modelling studies such as Bailey et al. (2005) suggest that accurate knowledge of heat budgets in the Labrador Sea is vital to properly constrain deep water formation. Floats are also excluded from the continental shelf, ice covered and most of the shelf areas. Moored observations provide sampling that is more frequent in time. Several long term moorings exist in the Labrador Sea with the German K1 mooring in the central Labrador Sea (2004-present) e.g. Avsic et al. (2006) and moorings nearer to the shelf break by Fisheries and Oceans Canada (e.g. Yashayaev & Loder, 2016). Ship cruises can provide sampling in higher spatial resolution, but they can be rather treated as snapshots in time and they are typically limited to summer season, meaning that the winter periods are undersampled. Satellites can provide higher spatial resolution of e.g. sea surface temperature at daily or higher frequencies, but cloud coverage (pervasive during the cold winter months) limits visibility in the infrared and visible range of the spectrum. In addition, subsurface data are required to assess the strength of wintertime mixing and to understand the export of newly convected water.

Gliders can help to close this observational gap because they can operate in winter conditions and can be directed to sample in particular areas of interest. Glider data quality is improving but to achieve more confidence in the data, glider observations should be coordinated with other platforms, as glider sensor payloads are limited by the strict power considerations of the platform. To target a particular oceanic process it is also important to separate the inherent smearing of time and space signals in glider data, given that they move at most at 25 km day^{-1} (e.g. Rudnick, 2016). In the Labrador Sea, gliders have been successfully deployed on several occasions (Hátún et al., 2007; Eriksen & Rhines, 2008; Frajka-Williams et al., 2009, 2014; von Oppeln–Bronikowski et al., 2021)

and they have shed new light on the dynamics in this region, particularly on winter cooling, mixing, density stratification and role of eddies, to name a few.

In this study, we deployed a glider in the wintertime into the Labrador Sea (Figure 1). The focus of the sampling was on understanding the wintertime exchange of heat and salt, in particular the role of transient processes such as eddies and storms for the mixed layer depth formation and ocean heat storage. This glider was stationed in the deep convection zone in the western part of the Labrador Sea (see Figure 1b). In this paper we address three questions:

1. To what extent do small scale processes contribute to the cycle of heat and salt exchange in this region and therefore the formation of LSW?
2. What are the dominant scales of water property evolution in the Labrador Sea?
3. In particular, do gliders offer critical information on scales below that offered by Argo floats?

2 Data and Methods

2.1 Glider Data

We deployed a Slocum 1000 m glider into the Labrador Sea during the Winter 2019-2020. The glider sampled the deep convection area highlighted by the <800 m mixed layer depth contours (Figure 1b). We use a similar geographic definition as in other studies in the area (see Yashayaev (2007); Yashayaev and Loder (2017)).In this study we present observations from January 15 to May 20, 2020. The glider sampled with a mean spatial resolution of 1.5 km and 2-hr between profiles (Figure 1a). The details of this mission are described in de Young et al. (2020), including the challenges and many lessons learned as part of this long-duration (7–month) mission in a harsh and remote environment.

The Slocum glider data were processed following basic quality control procedures recommended by the Australian National Facility for Ocean Gliders (ANFOG) Integrated Marine Observing System (IMOS) best practices document (Woo, 2019). The processed T-S profiles are shown in Figure 2. We converted raw glider data to level-1 and level2 data sets using the SOCIB toolbox (Troupin et al., 2015) following ANFOG/IMOS best practices. We used the ANFOG/IMOS QC manual for data flagging, linear interpolation of longitude and latitude, time vectors filling gaps, outlier detection, and spike removals. Profile identification and splitting was done using the pressure inversion method. Product profiles of T and S were bin-averaged on a 1 m depth grid going from 0 m to max profile depth (1020 m). Thermal lag was corrected with respect to T in pumped CTD cell following the standard correction from Morison et al. (1994) using 8 ml s^{-1} flow speed inside the conductivity cell. The exact procedure for glider pumped CTDs is described in the ANFOG/IMOS manual. Absolute salinity, conservative temperature, potential density are calculated with the TEOS10 toolbox (McDougall & Barker, 2011). Gridded profiles were corrected for up/downcast mismatch using RMS minimization described in the ANFOG/IMOS manual, median delay (T=2.39s^{-1}, C=2.05s^{-1}) was used for all variables. For the final data set we used a Savitzky-Golay filter for salinity (7 steps, 1st order) to remove occasional spikes in the lag corrected and up/downcast mismatch corrected profiles.

2.2 Ancillary Data

We used ERA5 global reanalysis (Hersbach et al., 2020) winds and surface forcing with 1-hr temporal resolution and 1/12° grid spacing resolution. Data were downloaded from the Copernicus Climate Data Store (CDS) website (Hersbach et al., 2018). We estimated the surface heat fluxes from ERA5 by including latent (Q_l) and sensible

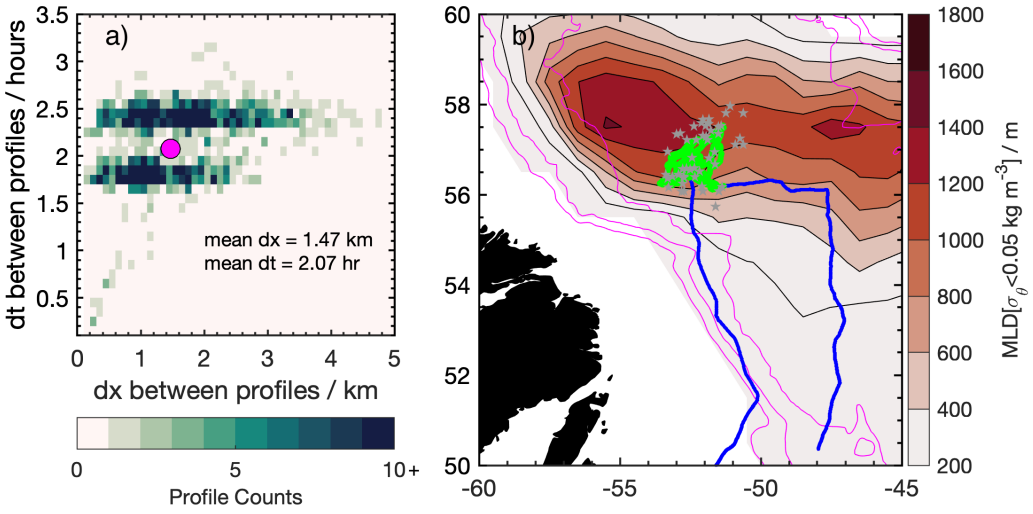

Figure 1. (a) shows the spatial and temporal resolutions between glider profiles with the pink dot indicating the mean. (b) Location of glider profiles (green from January 15 - May 15, 2020) and of Argo profiles (grey stars) taken over the same period and within 60 km of the glider profiles. Background color is the winter (January 1 - March 31) mixed layer depth extracted from the extended Roemmich-Gilson (Roemmich & Gilson, 2009) Argo climatology (2004-2020) based on the 0.05 kg m^{-3} density change criterion. Isobars (1000 m spacing) are superimposed in magenta.

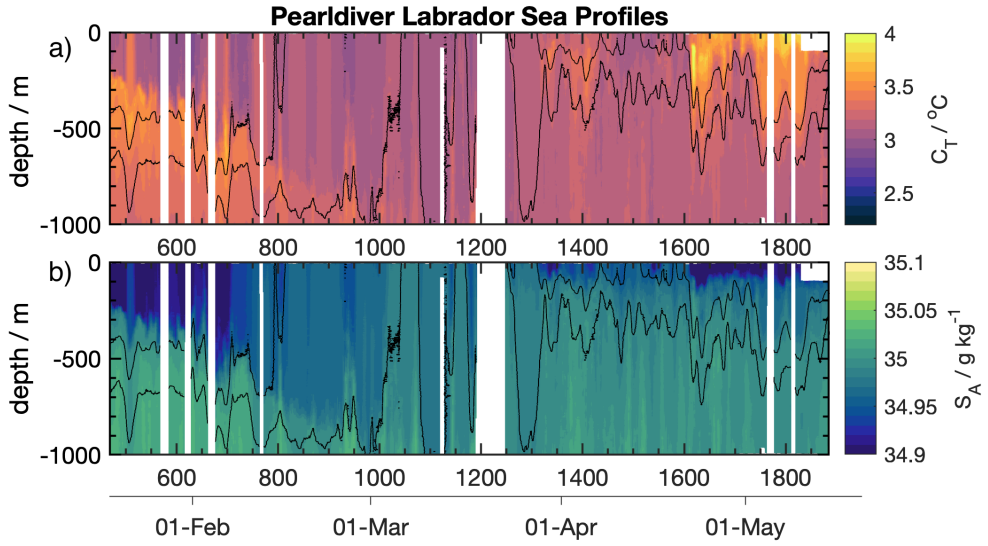

Figure 2. (a) T and (b) S profiles (x-axis is a profile number and the time) from the glider corresponding to the highlighted green track (Figure 1b) from January 15 to May 15, 2020. Gaps are periods when the glider was not sampling due to problems with the onboard computer. Contours of the 27.71 and 27.73 kg m^{-3} potential density surfaces are shown in black. Towards the end of April - beginning of May a strong freshening and warming is due to an eddy that trapped the glider for nearly 2 weeks.

(Q_s) turbulent heat fluxes, as well as the net longwave (Q_{lw}) and shortwave radiation (Q_{sw}). We calculated the net surface heat flux (Q_{net}) in W m^{-2} , where negative values indicate a net heat loss from the ocean to the atmosphere and positive values indicate a net heat gain by the ocean from the atmosphere:

$$Q_{net} = Q_l + Q_s + Q_{sw} + Q_{lw} \tag{1}$$

Argo data were extracted from Argo Global Data Assembly Centre (GDAC) (Argo, GDAC, 2000). We extracted all Argo profiles (total of 2678) from 2002 to 2020 between 44°W and 65°W and 44°N and 66°N. Data were checked for QC using the Argo DAC guide (Wong et al., 2020). Outliers were removed for T and S outside the ranges $-2 < T < 25$°C and $30 < S < 35.5$. For delayed time mode data, only data with quality flags of 1 or better were selected. In winter-spring 2019-2020, there were seven separate Argo floats present (WMO: 3901668, 4902395, 4902469, 4902471, 4902478, 4902481, 6902684) in this region within 60 km of the glider profiles during most of the glider sampling period. These floats collected a total of 48 profiles. The mean separation between profiles for the Argo floats (profiling every 10 days) was 55 km, compared to 1.5 km for the glider.

2.3 Mixed Layer Depth Estimation

We estimated the mixed layer depth using a threshold criterion of d= 0.01 kg m-3 density change for glider and Argo profiles, finding the depth Z_{MLD}, where $\Delta\rho = \rho(z(i)) - \rho(z = 10) < 0.01$ kg m^{-3}. We ignored profiles shallower than 10 m, because the glider was inflecting 12 m below the surface and because mixed layer depths during Jan-May were all greater than 10 m. The shallowest mixed layer depth we computed for the glider using this method was 30 m in April and the deepest was 1020 m, the maximum dive depth of the glider. The glider probably underestimated the MLD from Feb 20 to April 5 (Figure 3) as in this time the MLD likely exceeded 1000 m. Using this density threshold, we find MLD comparable with those reported in the literature (Yashayaev, 2007; Körtzinger et al., 2008; Yashayaev & Loder, 2016) for the Argo observing period . The choice of criterion or method has a large effect on calculated values of MLD as discussed and compared in Holte and Talley (2009). As an example, we found that MLD could vary between 373 m ($\Delta\rho$=0.01 kg m^{-3}) and 848 m ($\Delta\rho$=0.05 kg m^{-3}) for an identical T-S profile. Applying the hybrid method from Holte and Talley (2009) usually returned values close to those estimated with the d=0.01 kg m^{-3} criterion. A detailed overview and sensitivity analysis is beyond the scope of this study. We justified our choice of MLD density criterion based on how well our estimates aligned with those in the literature to provide a better comparison.

2.4 Vertical Heat and Freshwater Content

To estimate the Ocean Heat Content (OHC) per unit area (a = 1 m^{-2}), we followed Boyer et al. (2007) (their Equation 2),

$$OHC = a \int_{z_1}^{z_2} \rho_m C_p (T_c - T_m) dz \tag{2}$$

Here OHC is the ocean heat content (J / m^{-2}), ρ_m and T_m are the reference density (1027.3 kg m^{-3}) and temperature (3.2°C) for the upper Labrador Sea Water (uLSW) (Rhein et al. (2007) their Figure 4c), respectively. C_p is the heat capacity of seawater (4000 J kg^{-1} C^{-1}). We integrated temperature profiles for two layers 0-500 m and 500-1000 m, setting z_1 and z_2 appropriately for both Argo and glider profiles. In Boyer et al. (2007) they integrated in-situ temperature but we used conservative temperature T_c calculated from absolute salinity, in-situ temperature and pressure (McDougall & Barker, 2011).

To estimate the Freshwater Content (FWC), we followed the method of Florindo-López et al. (2020) (Equation 2), except that we are switching around the terms to interpret positive values as an addition of FWC (fresher) and negative removal of FWC (saltier). As before we integrate independently from z_1 to z_2, for both the top 0–500 m and intermediate 500–1000 m layer.

$$FWC = a \int_{z_1}^{z_2} \frac{\rho(S,T,P)}{\rho(0,T,P)} \frac{(S_m - S)}{S_m} dz \tag{3}$$

As above, ρ is the seawater density. We used (S) absolute salinity and not practical salinity as in the original method, as well as the reference Salinity (S_m) of 35 g kg^{-1} which is the mean salinity of the upper 1000 m of the study area from Jan 15-May 15, 2020 to look at the anomaly in salinity over the water column.

2.5 Correlation Scale Calculations

We use the glider data to estimate the correlation length scales of the observed T and S fields for each glider transect to investigate the spatial structure of dynamic events (eddies, convection, storms) during this period. This is difficult with the sparse Argo profiles, but we can use the higher resolution repeated glider tracks in each month to characterize T and S correlation lengths scales over the potential density layer where the new Labrador Sea water forms through the mixing of intermediate-depth and surface cooled waters (top 1000 m). To quantify the spatial scales, we used the definition of the autocorrelation function $r(k)$ following the results in von Oppeln–Bronikowski et al. (2021) for any isopycnal layer of interest.

$$r(k) = \frac{\sum_{t=1}^{N-k}(x_t - \bar{x})(x_{t+k} - \bar{x})}{\sum_{t=1}^{N}(x_t - \bar{x})^2} \tag{4}$$

Here x_t denotes measurements of T and S along with the isopycnal layer at step t, and $\bar{x}$ is the mean value along the spatial dimension k, N is the total number of samples. Before calculating the spatial correlation functions we average T-S data along the transect inside a particular isopycnal layer ($\pm$ 0.01 kg m^{-3}) and detrended the T-S data, to remove non-stationary spatial trends. Equation 4 then gives us the autocorrelation function as a function of lags. We use the lag at the first zero-crossing as the correlation length scale (see Supplement Figures S2 and S3). In our calculations we spatially reference the glider data to the westernmost measurements of the glider so that distances are consistent between transects.

3 Results

3.1 Argo-Glider Heat and Freshwater Content

We calculated the OHC and FWC from Argo and glider profiles following Equations 1 and 2, for two depth layers from 0-500 m and 0-1000 m. We did this for every glider and co-located Argo profile in the region. We chose these two layers to determine the difference and relative contribution of each layer to heat and freshwater change in the water column. ERA5 data have been extracted closest to the glider track positions (1-hr time steps).

The ERA5 surface heat fluxes (Figure 3a bars, black line) track the general cycle of cooling (-200 W m^{-2}) in winter (January - early April) with a gradual warming (200 W m^{-2}) towards spring (April-May) reported in other studies (Straneo (2006), their Figure 1a). The shift from predominantly cooling to warming is noticeable as well as a rather abrupt shift near the end of April after which cooling events subside, except a few events

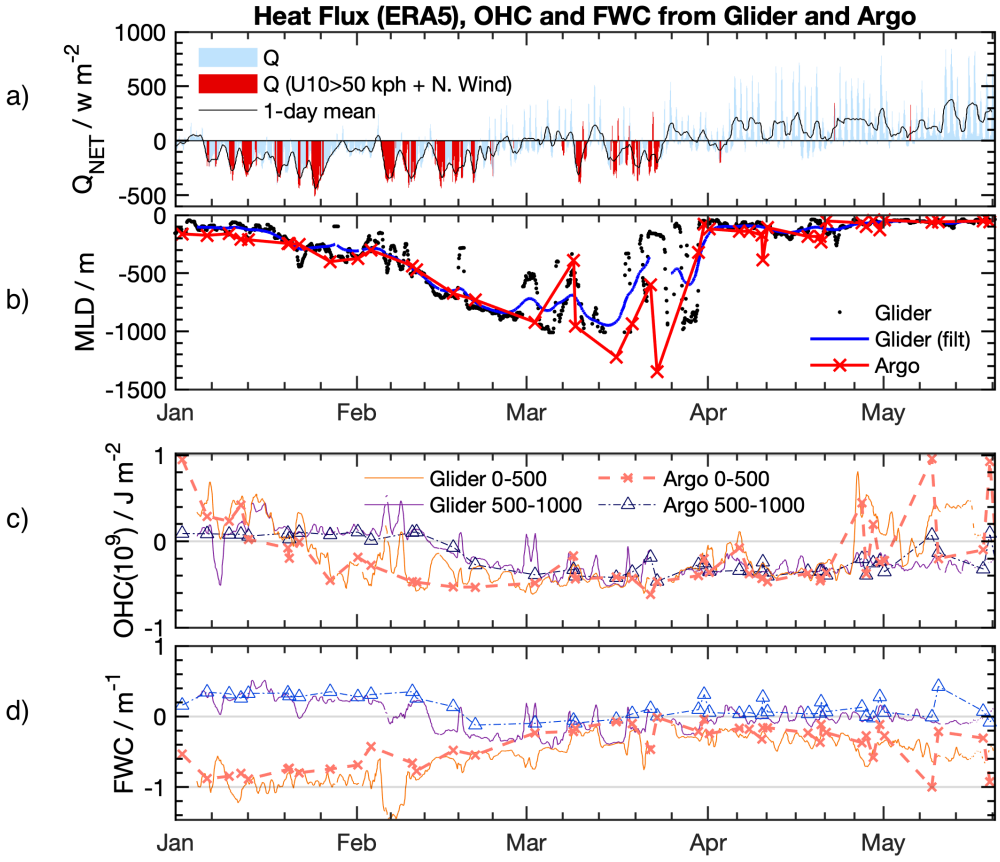

Figure 3. (a) Net heat flux from ERA5 with red shading for wind speeds from a northern direction in excess of 50 km hr-1 and (b) glider and Argo mixed layer depths. (c) and (d) OHC and FWC content calculated from glider and Argo profiles for the joint sampling period. OHC and FWC are shown for two depth layers from the surface to 500 m (orange) and 500-1000 m (bluish) with a glider (line) and Argo profiles (markers and dashed)

lasting only a few hours. Inside these phases of cooling and warming there is a lot of variability with sudden spikes of warming in excess of 700 W m^{-2} noticeable as deviation from the daily average (black line). Storm systems frequently track through the Labrador Sea from a Northern direction that import cold air and enhance cooling or so-called cold air outbreaks (Moore et al., 2014). We color-coded negative heat fluxes when the air was coming from a northern direction and winds were in excess of 50 km hr^{-1} and appear to be influenced by a 2 week time–scale as described by Sathiyamoorthy and Moore (2002). Overall the lowest heat fluxes in our data do not exceed -500 W m^{-2}. This is less than previously observed winter-minimums (-1500 W m^{-2}) in the vicinity (Lilly et al., 1999).

The time series of measured mixed layer depths (Figure 3b) reveal a deepening of the mixed layer during this period of heat loss, with estimated MLD from the glider and Argo floats agreeing well until March. After this time, the glider turnaround depth of 1020 m is too shallow to capture the full extent of mixing. During March, mixed layer depths from Argo profiles exceeded 1500 m, with the deepest measured mixed layer depth of nearly 1900 m deep near the end of March (Figure 3b). The onset of shoaling MLD is rather sudden (within 1 week) after which the MLD is generally less than 200 m. The

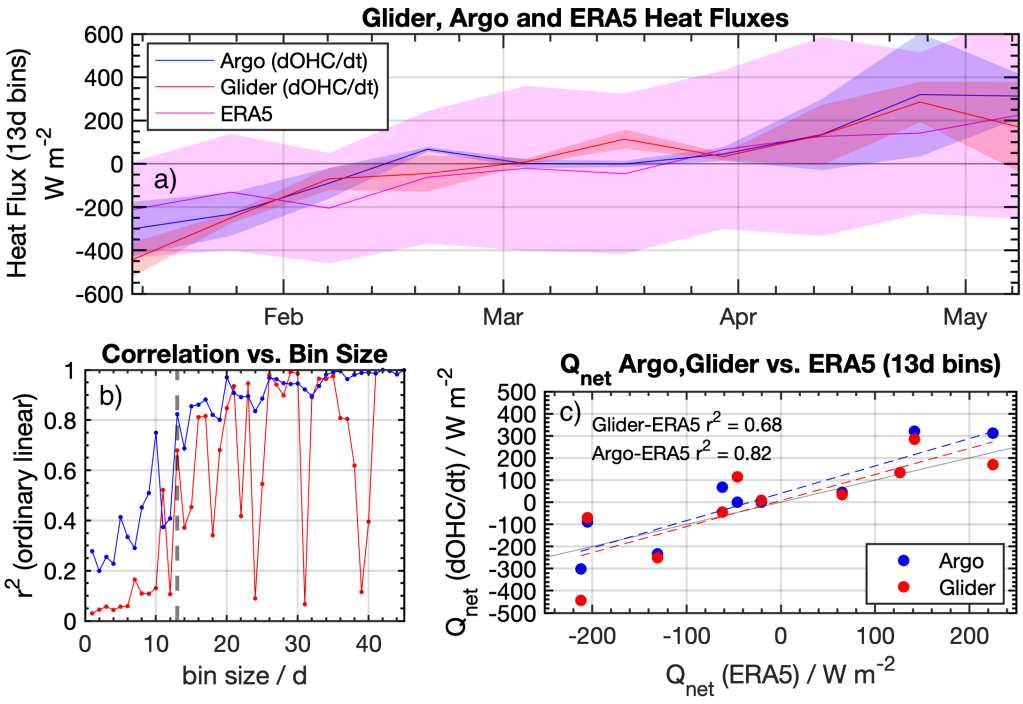

Figure 4. (a) Implied Argo, glider and ERA5 13-day averaged heat fluxes. Glider and Argo heat flux is the derivative of the OHC (0-500 m layer). Background shading is the upper and lower bounds based on the standard deviation from the bin averaging. (b) Correlation results Argo and Glider vs. ERA5 for different bin-sizes with 13-day bin size highlighted by vertical dashed black line. (c) Correlation of glider, Argo and ERA5 fluxes for the 13-day bin size. Line in the background shows 1:1 fit.

higher sampling resolution of the glider captures some spatio-temporal variability of the mixed layer depth not observed by the sparse Argo profiles. Filtering the glider data with a low-pass filter for time periods shorter than 3-days (blue in Figure 3b) removes those features from the glider record.

OHC provides a different measure of the intensity of watermass transformation than mixed layer depth (Figure 3c). In the near surface layer (0-500 m), the OHC started decreasing from the start of the record (January) reaching a minimum in the first week of February. In the intermediate depth 500-1000 m a decrease in OHC was only noticeable after Feb 10, reaching a minimum around March 1. OHC estimates from glider and Argo profiles coincide well, however the high temporal and spatial sampling of the glider captures much greater episodic variability compared to the Argo profiles. OHC in both layers becomes nearly equal after March. OHC at different depths are quite different in February when convection intensifies. This suggests that convection may start in the upper layer before affecting the deeper layer as expected from convection forced by surface heat flux.

On the other hand, FWC shows distinct differences between the two integrated layers. The top 500 m (orange, Figure 3d) is saltier compared to the mean reference salinity (35 g kg^{-1}), while the 500-1000 m layer (blue, Figure 3d) is initially fresher than the surface layer. As the mixed layer deepens, and the two layers mix, the FWC in the surface layer decreases (water becomes saltier) while the FWC in the deeper layer increases (water becomes fresher). The FWC of the two layers merges in March during the pe-

riod of the deepest mixing. Some short-duration events appear (1 m^{-1} drop in FWC for in the surface layer Feb 3-11) in the glider time series with the removal of FW on the order of 1 m^3 in the timespan of a day. These apparent salinifying events are associated with the glider passing through eddies with different water masses and FWC than the surrounding water. These salinity altering events extend to the bottom layer, pointing to their energetic nature.

We are interested in how well the sub-surface glider and Argo data resolve surface driven processes such as wind-driven surface mixing. We expect that by calculating the correlation between surface fluxes (ERA5) and inferred surface fluxes from the changes in OHC (Argo and glider) the residuals of this correlation may be partly explained by wind-driven surface mixing. To estimate implied fluxes from the change in observed ocean heat content $Q_{net,obs}$, we take in Figure 4a the derivative in time

$$Q_{net,obs} = dOHC/dt \tag{5}$$

where $dOHC$ is the difference of OHC over the time interval dt for both observed profiles. Here we take the surface layer (0-500 m) as our best estimate with surface fluxes from ERA5. We bin average results to a common time scale between the Argo and glider observations. Argo profiles are spaced approximately every 10–11 days. The Argo data is sparse and 10-days is the practical limit over which we can compare surface processes with Argo data. Indeed, the correlation between ERA5 and implied heat fluxes from Argo reveal a spike in correlation for 10 day averaging and a steep drop for values smaller than that (Figure 4b). However, this story is more complicated for correlation between ERA5 and glider data. For small averaging windows (<10 days) the data do not agree well with $r^2 < 0.2$. On 13-day time scales (Figure 4c) we find that Argo ($r^2 = 0.82$) and glider data ($r^2 = 0.68$) are in overall agreement. During this averaging interval the glider covered approximately 154 km. Thereafter, the correlation between ERA5 and Argo improves steadily the larger the window size and on monthly scales (30-day) they agree over 90%. This makes sense given that increasing window size filters out small scale variability and that ERA5 data assimilates data from Argo. In contrast, larger averaging windows do not necessarily produce better correlation between implied heat fluxes from the glider data and ERA5. There are spikes and drops for different windows with 25-day rising $r^2 > 0.8$ and 31-day dropping $r^2 < 0.2$.

3.2 Winter 2020 Convection and Correlation Scales

The Argo time series goes back to 2002, but significantly more profiles are available from 2012. Yashayaev and Loder (2016) (their Figure 4d) show a trend of increasing density for the thickest density layer from 2012-2016 with the 2016 Labrador Sea water being denser and colder than previous convection classes such as the LSW 1994, 2008 classes (Yashayaev, 2007; Yashayaev & Loder, 2016). We extend in Figure 5 the analysis from (Yashayaev & Loder, 2016) to the time of the glider observations to provide context for the high resolution glider observations and put them into the context of other studies.

We use the Argo profiles in the region near the glider observations with a box similar to Yashayaev and Loder (2016) (their Figure 1) from 2011 to 2020. We bin average all Argo profiles inside this spatial box in 14 day and 0.005 kg m^{-3} density bins (Figure 5a). A figure showing all Argo floats selected for the average is given in the supplement (see Supplement, Figure S1). Different from Yashayaev and Loder (2016) we use the potential density to 0 dbar (σ_0 instead of σ_1). The result in Figure 5a shows an increasing trend in LSW density from 2012 to 2017, similar to the results in Yashayaev and Loder (2016). The period of 2017 to 2018 shows density of LSW in the convective zone

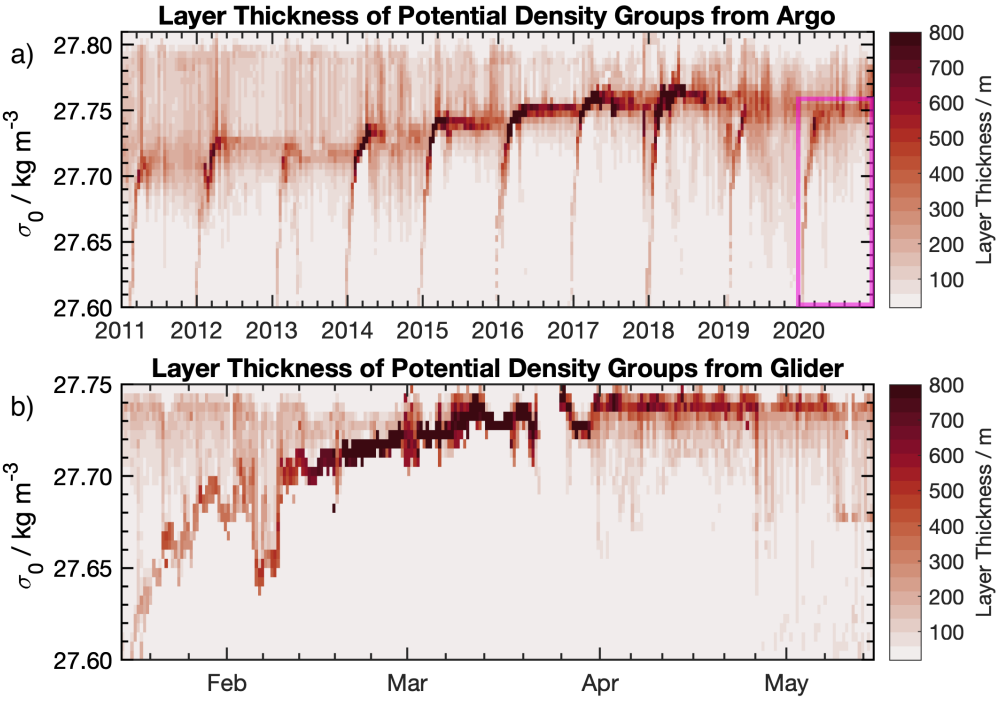

Figure 5. (a) Isopycnal layer thickness diagram is broken down by year from Argo data (2012-2020) in 14-day by 0.005 kg m^{-3} bins. Box indicates range of glider observations. (b) Layer thickness for each month for glider observations in the Labrador Sea in 2020 in bins of 12-hr and 0.005 kg m^{-3}.

nearly constant and then decreasing in 2019-2020. The onset of convection in 2019-2020 appears to be also later compared to the previous five years.

Convection in 2020 from Argo data in the glider observing period (pink box in Figure 5a) shows similar convection intensity to 2013 (Figure 5a) albeit with less thickness observed in the density layers. The glider observations for the period of winter 2019-2020 (Figure 5b) show that the volume of density groups exhibit variability not seen by Argo in terms of thickness of density layers and the variability of the density layer thickness. There is an event of lighter water occupying a larger depth range from a salinifying but warm feature (see Figure 3c-d), which later analysis (see Figure 8) shows to be an eddy. The glider record stops at 1000 m and misses the densest layers of convected water in March ($\sigma_0 > 27.75$) but shows well mixed layers for the entire water column occupying the same density. The glider data also shows that events like an eddy, that was detected in February, results in water with different density than otherwise observed in the record. The onset of spring and end of convection shows gradual spread of density layer thickness as the water column re-stratifies.

One of the key questions around the heat and freshwater calculations (Section 3.1) concerns the spatial homogeneity in the obtained results. Here we break the glider data into individual transects and calculate the spatial correlation length scale as per methods (Section 2.5). A sample autocorrelation function for an isopycnal is given in the supplement (Figures S2,S3). We repeat the analysis for every isopycnal group observed by the glider range from 27.65 to 27.75 kg m^{-3} to find the correlation scales. The glider managed to do 16 transects during the 5-month period in the central Labrador Sea, each at least 90 km long and lasting a week, with the majority 150-200 km long and lasting two

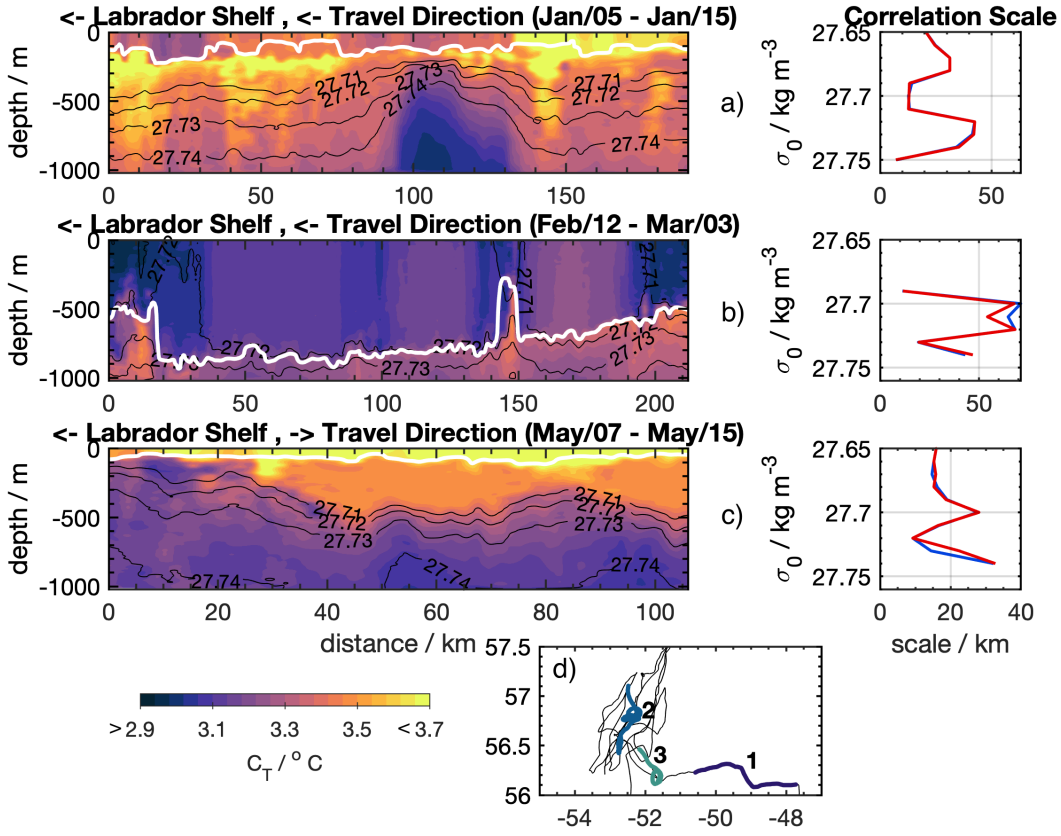

Figure 6. (a), (b), (c) Glider sections with eddy or ventilation events (left side) and corresponding correlation scales (right hand side) for T(blue) and S(red). Note the potential y-axis is reversed to align with the glider transects. White contour indicates the mixed layer depth, and black contours the potential density contours spaced every 0.01 kg m^{-3}. (d) Inset map shows the individual tracks used for the glider section analysis.

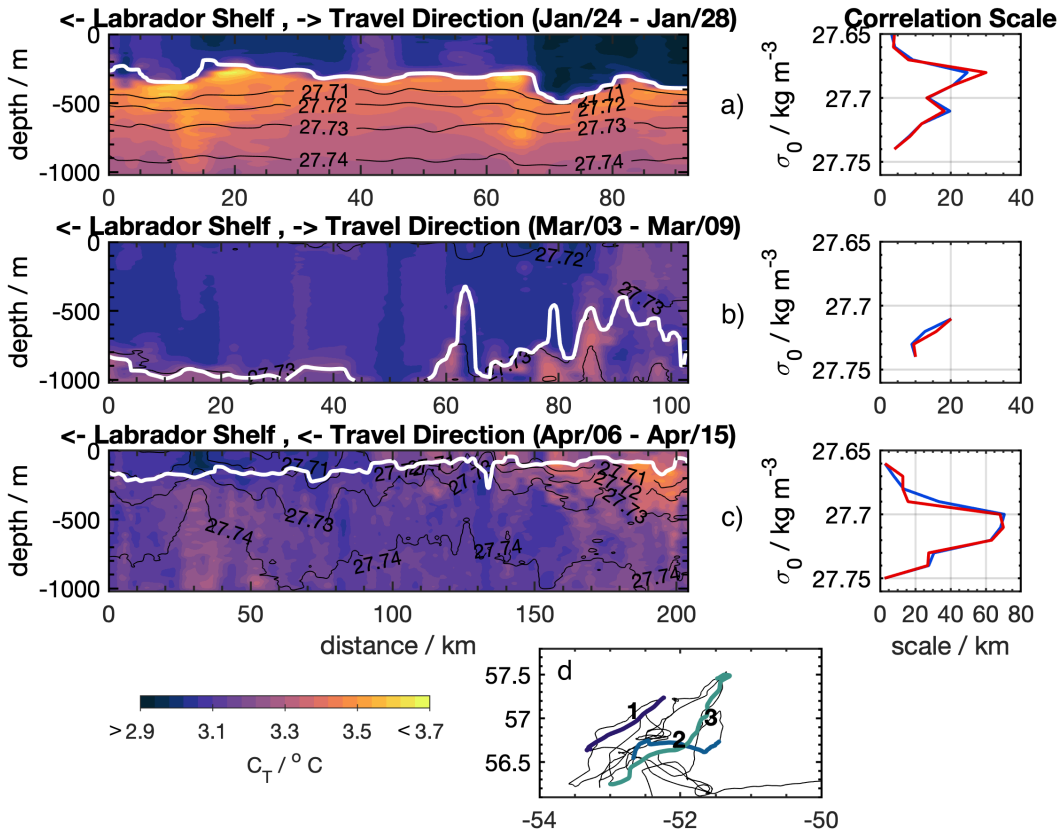

Figure 7. Same as Figure 6 but for the glider sampling transects without eddies.

weeks. There were sections containing several eddy signatures from either the same or different eddies (Figure 6) and there were sections that contained no apparent eddies (Figure 7). The sections were picked for the stages of convection with the upper panel corresponding to the preconditioning, middle panel with active convection and lower panel with re-stratifying post convection. The presence of eddies influences the correlation length scale, though it is not possible to accurately estimate the eddy size because of the slow speed of the glider, causing spatial aliasing. For example the uppermost panel (Figure 6) shows an early cyclonic eddy event around 110 km, the middle panel is the edge (150 km) of an eddy smearing the glider signal and the bottom panel is an energetic anti-cyclonic eddy centred at 60 km that trapped the glider for nearly two weeks from end of April to middle of May. The corresponding correlation scales of these sections containing eddies appear to show that the density layers corresponding to the lens of the eddy appear to increase. To properly determine the size of the eddy it would be better to attempt to estimate the dynamic height from the glider data and attempt to correspond these observations with another independent reference like single track satellite altimetry data. The temperature and salinity scales (Figure 6, 7) generally coincide with each other.

We summarize the correlation scale analysis (Figure 8) over the entire record with bars identifying sections sampling an eddy. The mean mixed layer depth for each section is the green horizontal line. The time bar is scaled to fit the sections into equal bins and is slightly distorting the timing of the events. Overall, the correlation scales within the mixed layer (above the green line, Figure 8) are smaller than 15 km unless eddies are detected. This confirms a result of von Oppeln–Bronikowski et al. (2021) where the glider sections were uniform in T and S, sampled in October and November, showing monthly

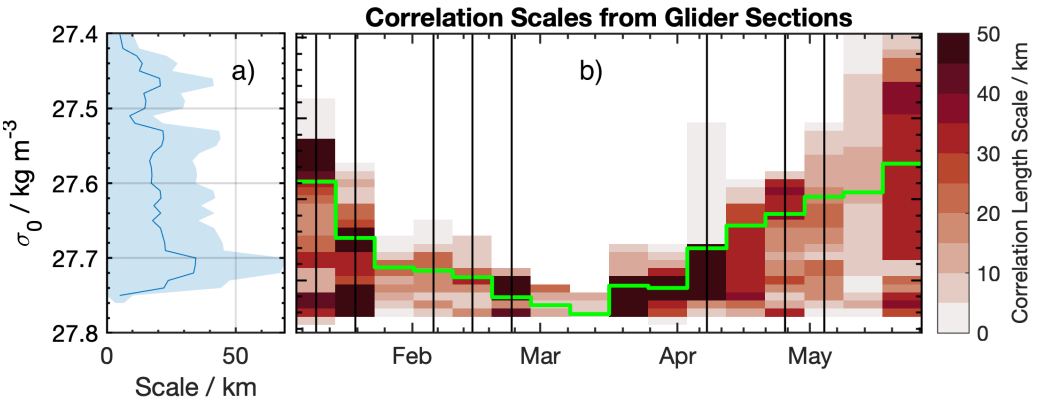

Figure 8. a) Length scales of temperature averaged for all glider sections over the entire record, broken down by isopycnal group observed in the glider record. Shading is ± 1 STD (b) Length scales for each section in each density bin (0.01 kg m^{-3}). The green line is the mean mixed layer depth isopycnal in the period the sections were surveyed by the glider. Vertical lines indicate when an eddy was present in the surveyed sections. Note the y-axis (σ_0) is oriented from shallower (lighter) to deeper (denser) water.

averaged scales around 10–15 km. In general, our data point to a non-heterogenous state of mixing and T and S variability in the Labrador Sea before, during and after convection.

These results suggest that there is significant spatial variability at scales much shorter than those sampled by the Argo floats. It is noteworthy that the scales observed are smaller than what would be captured in CMIP style models (Hasumi, 2014) used in climate prediction scenarios (IPCC). Given the importance of convection and ventilation to longer climate timescales (storage of carbon in the deep ocean Khatiwala et al. (2013)) our results suggest that important processes happening on these scales are also not captured in these simulations.

4 Discussion

4.1 Difference in OHC and FWC between Glider-Argo Observations

Based on the correlation scale analysis of the previous section, it becomes apparent that the processes that drive T and S variability are not heterogeneous. The extent to which this variability is captured by Argo floats is not entirely clear given that the sampling does not allow us to repeat the same analysis as used on the glider data. Instead, we focus again on the OHC and FWC calculations from Section 3.1, to investigate the role eddies play on the overall OHC and FWC measured from the glider and Argo floats.

For a robust comparison between Argo and the glider, we bin averaged the profile data for each month in Figure 9. The OHC and FWC averages ± their standard errors ($STD/\sqrt{n}$) with STD meaning the standard deviation and n the number of independent samples) are displayed in Figure 9. The glider covered a total distance ranging from 405-493 km per month. The correlation length scale analysis (Figure 8) showed that the glider data (monthly averages) are correlated within 19-26 km of the zero-crossings and therefore are not independent within/below this distance. This suggests the presence of 15-23 independent samples, n, in each section. We estimate the number of independent

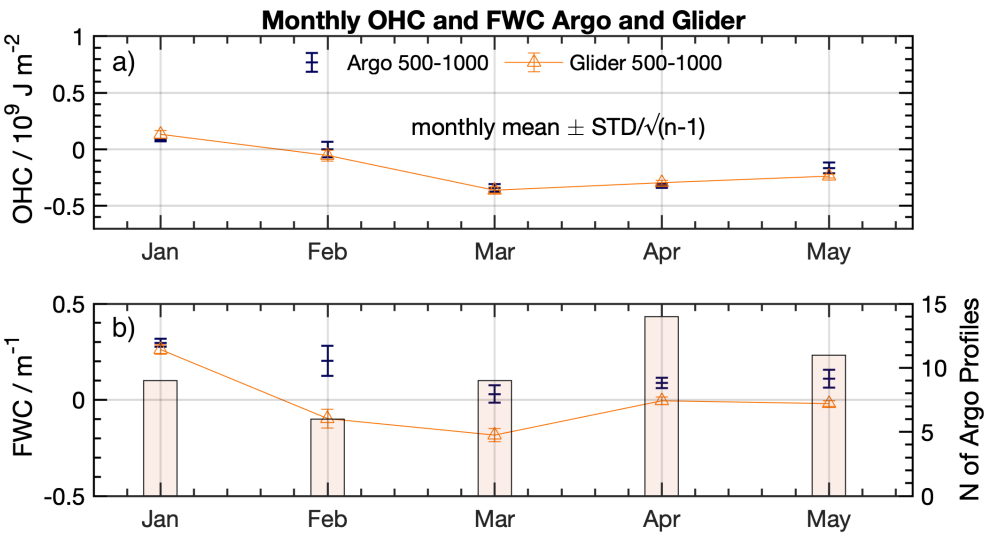

Figure 9. Comparison of monthly averaged OHC (b) and FWC (c) calculated with Argo (dark purple) and glider (orange) profiles in the subsurface 500-1000 m layer, with error bars indicating +/- 1 standard errors. Bars in (b) show the number of Argo profiles used for the monthly average.

Argo profiles with 6 to 14 profiles sampled each month. Given that the distance between float profiles averaged around 55 km, compared to just a few km for the gliders (Figure 1 1, and the low mean correlation scales (from the glider), we assume that each profile is independent ($n = 6-14$). On average between two profiles over 10 days a float would travel 55 km. We focus on the deeper layer 500-1000 m to look at subsurface (Jan-Feb, Apr-May) effects below the mixed layer. From the correlation scale analysis, we know that the subsurface correlation scales are larger than at the surface, providing a more robust comparison between the two platforms.

Comparing the Argo and glider data (Figure 9), we find that the deep-layer (500-1000 m) cooled and freshened during the period of convection. While Argo and glider monthly OHC are in agreement, FWC are not, with the exception of January. What is causing this difference of up to a maximum of 0.3 m^{-1} in FWC in February and minimum 0.035 m^{-1} in January in the subsurface intermediate depth layer between Argo and glider observations? February is the month of the lowest number of Argo float observations (6). There appears to be a decrease in difference between FWC estimation with an increase in monthly Argo observations (maximum of 14 in April, FWC difference 0.0939 m^{-1}). Accurate knowledge on surface and subsurface salt fluxes in this region is critical to properly represent mixed layer dynamics. From the previous section on correlation scales we also know that it was during these months that the glider encountered the majority of eddy events though eddies were also present in January. It could be that these observed eddies have an influence on the overall FWC and that the Argo data may not capture all of this variability.

Given the disagreements in the monthly FWC data between Argo and glider, what is the importance of the small scale variability in the data vs data averaged over a time period like 10 days? If we subsample the glider data to Argo spacing of 10 days and compare this with the glider data averaged in 10 day bins we can investigate how much variability is missed by averaging vs an instantaneous representation given by the denser sampling of the glider (Figure 10). This gives a sense of how important dense sampling could

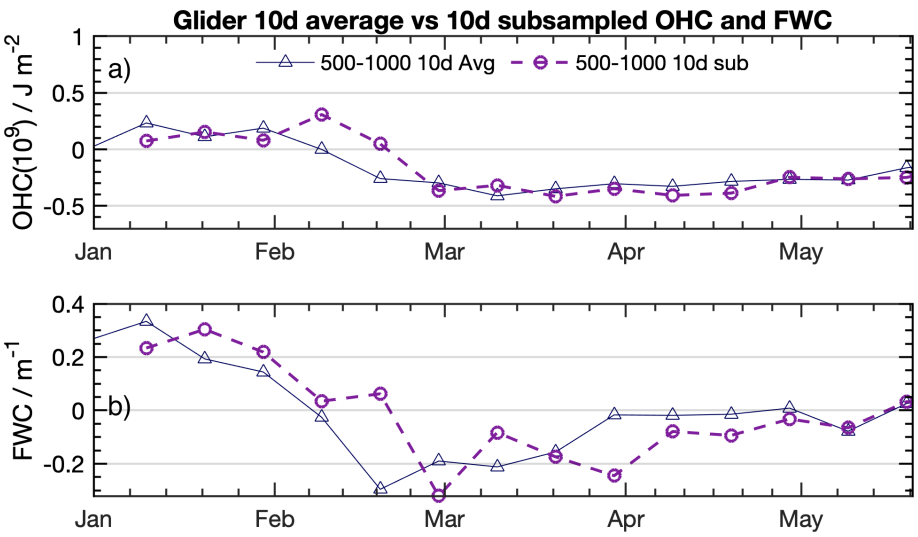

Figure 10. (a) Comparison of 10 day averaged glider OHC and (b) FWC vs 10 day subsampled data (approximately Argo sample spacing).

be. Looking at the result we see that the glider data subsampled and averaged are overall in good agreement, but that in months with increased eddy activity (February and May) there are differences of up to 50% between FWC and OHC subsampled vs averaged data.

4.2 Importance of Eddies on Heat and Salt Budget

From the previous section, it appears that Argo floats and glider data estimate similar monthly heat content means in the lower-layer. In contrast , there are differences in FWC between the two data sets, possibly due to the presence of eddies that are only detected with the spatio-temporal resolutions of glider measurements whereas Argo floats can sample within an eddy but their resolutions are too sparse to fully resolve the scale and energy of these events. The glider data show a non-heterogenous state with regards to the spatial structure of T and S important for our understanding of air-sea gas exchange, subduction and mixing.

We describe our idea of the observations and dynamics in Figure 11. The diagram shows Argo profiles and the glider trajectory inside a sampling box 200 by 100 km wide corresponding with the spatial coverage of the observation (see Figure 1b). There are eddies representing small-scale features throughout the sampling box as well as convection driven by both surface and eddy heat and freshwater fluxes. The glider encounters the eddies on several passes, while the Argo floats measure the large-scale process well, but do not resolve the smaller-scale eddy dynamics associated with the eddy. In Section 4.1 we estimate that the difference in glider and Argo OHC is small (within a standard error) but that differences in FWC can reach up to 0.3 m^{-1}. For some of the glider transects it is clear that it was the same eddy that was measured as the glider passed through the same T-S signature when it turned around. A total of 6 eddies were sampled by the glider. Our result of increased eddy activity in May aligns with other studies (Körtzinger et al., 2008; Fischer et al., 2018) which point to increased eddy kinetic energy in spring time following the tail of convection. Other studies (Chanut et al., 2008; Rieck et al., 2019) have also shown eddy events in the period during fall and winter. In addition, the glider

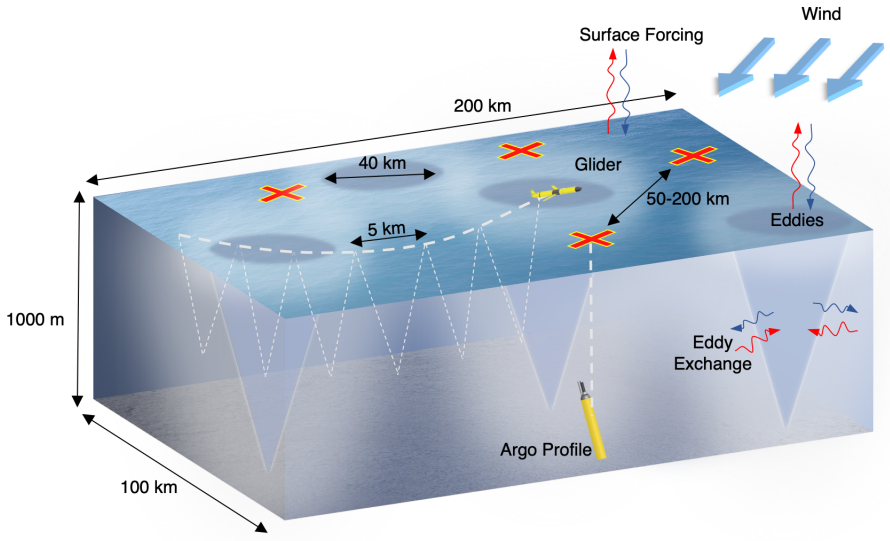

Figure 11. Schematic diagram of example glider sampling in the Labrador Sea together with Argo float profiles and eddies.

likely sampled the signal of convective mixing cells but their scales of meters to a few km are likely too small to be reliably sampled by the glider.

An open question remains around the relative contribution of freshwater due to eddies prior and after convection in terms of their impact on the onset of convection and restratification. A few studies have pointed at eddies and their role in modulating OHC and FWC in the Labrador Sea (Chanut et al., 2008; Hátún et al., 2007). We use our comparison between glider and Argo FWC and our eddy passes to address the importance of eddies over the whole basin using a simple scaling approach with the dimensions provided by the glider sampling. The approximate area of the glider sampling with Argo profiles is a box of 200 by 100 km, with 48 Argo profiles over the time from January to May (Figure 3). The glider did 16 passes along the 200 km corridor with 8 eddy events in all the transects completing on average 420 km per month. If we assume that eddies (approximately 40 km wide) are equally distributed and that the glider was managing the same section, the glider should have sampled an eddy approximately 50% of the time or every second pass through the 200 km corridor. We recognize that this is a crude assumption given that the eddy detection is not distributed equally every month. For the months with eddies, 20% (80 km / 420 km = 20%) of the total distance sampled by the glider spanned through at least one eddy. If we ignore issues around the glider sampling, we can approximate that 20% of the box area could have been occupied by eddies at any given time. In the previous section, we discussed the possibility that the start in FWC subsurface discrepancy between glider and Argo could partly be due to eddies. We therefore apply this area scaling directly to the difference in observed monthly FWC to work out an approximate contribution of eddies to FWC in the Labrador Sea using 300 km radius of convection region (Lilly et al., 2003). Using February as an example of strong eddy activity, we found a difference of 0.3 m^{-1} FWC between Argo and glider. We conclude that eddies could possibly contribute up to 4.2 m^{-1} FWC for the entire basin in that month. It would be interesting to see how our results compare against modelling studies. This could help to pinpoint discrepancies between models and observations, as well as help to understand the sources and sinks of freshwater in the Labrador Sea, which is an ongoing question (Aagaard & Carmack, 1989; Zhang et al., 2021). We note that the number of Argo profiles in winter is lower compared with the summer (see Supple-

ment, Figure S1), and that the glider moves slowly and likely not sampling the area well enough to confidently isolate the eddy contribution. Therefore, this exercise is more of a thought experiment but could help inspire the sampling strategies of future glider missions in the region.

5 Conclusions

In this study we presented winter time observations of heat and freshwater content and mixing in the Labrador Sea from Argo floats and a glider. In the Introduction, we posed three main questions for this paper: (1) To what extent do small scale processes contribute to the cycle of heat and salt exchange in this region and therefore the formation of LSW? (2) what are the dominant scales of water property evolution in the Labrador Sea? and (3) do gliders offer critical information on scales below that offered by Argo floats? Here we summarize the results and discussion as well as offer a future outlook on glider observation needs in the Labrador Sea.

We examined OHC and FWC for Argo and glider observations and found that unsurprisingly the glider exhibits a lot of small-scale energetic structure that is not seen by the coarser sampling Argo floats. These distinct events occur due to eddies and hence the question on the importance of the small scale structure is in part a question on the role of eddies for FWC and OHC in this region. The glider encountered a number of salinifying events which are associated with the glider passing through eddies with different water masses and FWC than the surrounding water. These salinity altering events extend to the deep (500-1000 m) layer, pointing to their energetic nature. Filtering the glider data by a 3-day low-pass filter removes the small–scale variability and most of the eddy signal. To answer the question to what extent these small scale processes contribute to the overall OHC and FWC in this region is difficult by the fact that we do not have enough glider data for a full year and not enough independent measurements of a field with eddies and without. From our discussion in Section 4.2 we think that eddies may play a significant role in redistributing OHC and FWC in the Labrador Sea. Similar conclusions are offered by eddy–resolving modelling studies that consider these contributions (Yeager et al., 2021). We further underline this point, comparing the three heat flux datasets (ERA5, Argo and glider derived implied heat fluxes) we find that the correlation between glider and Argo implied surface heat fluxes and ERA5 are dependent on window averaging. For the glider it appears that the spatial scales may impact the correlation scales. The more widely distributed Argo floats on the other hand show good agreement with ERA5.

Convection in the Labrador Sea in winter 2019–2020 was weaker than the previous year. The maximum MLD from Argo profiles reached nearly 2 km based on individual profiles. Though overall the volume of LSW formed during this year convection season was less than in the previous year's winter season (2018–2019). The deepening of MLD was rather gradual (Jan-March) but the end of convection was very abrupt (March 31–April 1). For the FWC and OHC calculations we broke the data into two separate layers: a surface (0-500 m) and a deep (500-1000 m) layer. There is a distinct separation in the two layers in January–February between FWC and OHC prior to convection (March). The merging of OHC and FWC for the top and deep layer is rather sudden, even though MLD changes are gradual. The end of convection and change in MLD is very dramatic occurring in a matter of days as evidenced by both data-sets. The ERA5 surface heat flux show that the end of convection is preceded by a week of weak warming (100 W m^2). These observations suggest convection is largely driven by surface heat fluxes. From the glider high-resolution transects we estimated the correlation length scales and find that the T and S structures exhibit a lot of heterogeneity due to the aforementioned eddy events. On average, spatial scales are small on the order of 15-20 km in agreement with previous glider experiments in the region (von Oppeln–Bronikowski et al., 2021). However, eddies have a significant influence on the spatial structure increasing length

scales to 40-50 km. We note several limitations to our approach. The glider only managed to sample one transect about twice a month. The slow speed likely aliased the space and time variability in the record. We limit the influence of aliasing in our assumption of spatial snapshots of the sections by detrending the data and working on isopycnal coordinates.

Monthly averages in FWC show significant differences between platforms during February, when eddy sampling by the glider was highest. We estimate,based on the discrepancy in FWC between Argo and glider data, that eddies could potentially play a significant role. Ignoring limitations of the glider data, we estimate that up to 4 m^{-1} of FWC change could be attributed to eddies for the entire Labrador Sea. The lack of comparable datasets limits how far we can push this result or allow us to further test our results. The Argo floats probably then sample the field in sufficient spatial density and coverage that they adequately sample the mean state of the Labrador Sea and so for bulk estimates do a good job of how has the Labrador Sea changed but do not give further insight into why. Gliders reveal a more detailed look at eddies which is important for understanding their role towards the bigger system of the Labrador Sea. Future glider missions could sample the region more densely to improve our understanding of the lasting influence of these eddies on the region. This is not possible to do with a single glider since the gliders are too slow to repeatedly and effectively sample such a large region.

Our results do not have a definitive answer as to the role of eddies, but rather offer another glimpse (see e.g. Hátún et al., 2007) that eddies might play an important role and that the role of the interior of the Labrador Sea towards pathways of watermasses is not yet sufficiently well understood. A recent paper by (MacGilchrist et al., 2021) point to the boundary as important for driving subduction and hence export and not the interior, however those results do not consider eddies. An observing strategy targeting both the export at boundaries and a way to track eddies is needed. We are planning to do a follow up long duration glider sampling experiment in the Labrador Sea with several glider sampling near the boundary current, flying along the boundary current to observe subduction as well as gliders offshore from the boundary current tacking snapshots of eddies that propagate into the interior of the Labrador Sea. The goal of this study would be to quantify the ideas in MacGilchrist et al. (2021) as well further analyze the contribution of eddies to FWC and OHC in the Labrador Sea. To properly disentangle the role of eddies, eddy tracking is needed which would relay on novel tools for glider navigation and remote sensing from satellites.

Data Availability

Processed glider data have been archived on SEANOE (`https://www.seanoe.org/data/00681/79349/`) as part of the Memorial University glider data repository (von Oppeln-Bronikowski et al., 2021). Argo data were collected and made freely available by the International Argo Program (Argo, GDAC, 2000) and the national programs that contribute to it (`https://argo.ucsd.edu,https://www.ocean-ops.org`). The Argo Program is part of the Global Ocean Observing System. ERA5 (Hersbach et al., 2018) 1-hr single level data were accessed from Copernicus Climate Data Store (CDS) (`https://cds.climate.copernicus.eu/cdsapp#!/dataset/reanalysis-era5-single-levels?tab=form`).

Acknowledgments

We are grateful to Fisheries and Oceans Canada for supporting our research and allowing us to join the AZMP Fall cruise in 2019 on the RRS James Cook. We are especially grateful to Chief Scientist Stephen Snook without whom the deployment would not have been possible. We thank Mark Downey for help in deploying and recovering gliders. Funding for the HOTSeALS project came from the Ocean Frontier Institute Module B Au-

diting the Northwest-Atlantic Carbon Sink. EFW, IG and LC acknowledge support from the Horizon 2020 TERIFIC project (grant agreement 803140).

References

Aagaard, K., & Carmack, E. C. (1989). The role of sea ice and other fresh water in the Arctic circulation. *Journal of Geophysical Research: Oceans*, *94*(C10), 14485–14498.

Argo, GDAC. (2000). *Argo float data and metadata from global data assembly centre (Argo GDAC)* [Dataset]. doi: 10.17882/42182

Avsic, T., Karstensen, J., Send, U., & Fischer, J. (2006). Interannual variability of newly formed Labrador Sea Water from 1994 to 2005. *Geophysical Research Letters*, *33*(21).

Bailey, D. A., Rhines, P. B., & Häkkinen, S. (2005). Formation and pathways of North Atlantic Deep Water in a coupled ice–ocean model of the Arctic–North Atlantic Oceans. *Climate dynamics*, *25*(5), 497–516.

Boyer, T., Levitus, S., Antonov, J., Locarnini, R., Mishonov, A., Garcia, H., & Josey, S. A. (2007). Changes in freshwater content in the North Atlantic Ocean 1955–2006. *Geophysical Research Letters*, *34*(16).

Chanut, J., Barnier, B., Large, W., Debreu, L., Penduff, T., Molines, J. M., & Mathiot, P. (2008). Mesoscale eddies in the Labrador Sea and their contribution to convection and restratification. *Journal of Physical Oceanography*, *38*(8), 1617–1643.

Clarke, R. A., & Gascard, J.-C. (1983). The formation of Labrador Sea water. Part I: Large-scale processes. *Journal of Physical Oceanography*, *13*(10), 1764–1778.

Desbruyères, D. G., Mercier, H., Maze, G., & Daniault, N. (2019). Surface predictor of overturning circulation and heat content change in the subpolar North Atlantic. *Ocean Science*, *15*(3), 809–817.

de Young, B., Frajka-Williams, E., von Oppeln-Bronikowski, N., & Woodward, S. (2020). Technicalities: Exploring the Labrador sea with autonomous vehicles. *The Journal of Ocean Technology*, *15*(3), 134–139. Retrieved from `http://nora.nerc.ac.uk/id/eprint/528776/`

Eriksen, C. C., & Rhines, P. (2008). Convective to Gyre-Scale Dynamics: Seaglider Campaigns in the Labrador Sea 2003–2005. In *Arctic–Subarctic Ocean Fluxes* (pp. 613–628). Springer.

Fischer, J., Karstensen, J., Oltmanns, M., & Schmidtko, S. (2018). Mean circulation and EKE distribution in the Labrador Sea Water level of the subpolar North Atlantic. *Ocean Science*, *14*(5), 1167–1183.

Florindo-López, C., Bacon, S., Aksenov, Y., Chafik, L., Colbourne, E., & Holliday, N. P. (2020). Arctic Ocean and Hudson Bay freshwater exports: New estimates from seven decades of hydrographic surveys on the Labrador Shelf. *Journal of Climate*, *33*(20), 8849–8868.

Frajka-Williams, E., Rhines, P. B., & Eriksen, C. C. (2009). Physical controls and mesoscale variability in the Labrador Sea spring phytoplankton bloom observed by Seaglider. *Deep Sea Research Part I: Oceanographic Research Papers*, *56*(12), 2144–2161.

Frajka-Williams, E., Rhines, P. B., & Eriksen, C. C. (2014). Horizontal stratification during deep convection in the Labrador Sea. *Journal of Physical Oceanography*, *44*(1), 220–228.

Gascard, J.-C., & Clarke, R. A. (1983). The formation of Labrador Sea Water. Part II. Mesoscale and smaller-scale processes. *Journal of Physical Oceanography*, *13*(10), 1779–1797.

Gelderloos, R., Katsman, C. A., & Drijfhout, S. S. (2011). Assessing the roles of three eddy types in restratifying the Labrador Sea after deep convection. *Jour-*

nal of Physical Oceanography, *41*(11), 2102–2119.

Hasumi, H. (2014). A review on ocean resolution dependence of climate biases in AOGCMs. *CLIVAR Exchanges*, *65*, 7–9.

Hátún, H., Eriksen, C. C., & Rhines, P. B. (2007). Buoyant eddies entering the Labrador Sea observed with gliders and altimetry. *Journal of Physical Oceanography*, *37*(12), 2838–2854.

Hersbach, H., Bell, B., Berrisford, P., Biavati, G., Hornyi, A., Muoz Sabater, J., ... Thpaut, J.-N. (2018). *ERA5 hourly data on single levels from 1979 to present* [Dataset]. Retrieved 2021-10-14, from `https://cds.climate.copernicus.eu/cdsapp#!/dataset/reanalysis-era5-single-levels?tab=form` doi: 10.24381/cds.adbb2d47

Hersbach, H., Bell, B., Berrisford, P., Hirahara, S., Horányi, A., Muñoz-Sabater, J., ... others (2020). The ERA5 global reanalysis. *Quarterly Journal of the Royal Meteorological Society*, *146*(730), 1999–2049.

Holte, J., & Talley, L. (2009). A new algorithm for finding mixed layer depths with applications to Argo data and Subantarctic Mode Water formation. *Journal of Atmospheric and Oceanic Technology*, *26*(9), 1920–1939.

Khatiwala, S., Tanhua, T., Mikaloff Fletcher, S., Gerber, M., Doney, S., Graven, H., ... others (2013). Global ocean storage of anthropogenic carbon. *Biogeosciences*, *10*(4), 2169–2191.

Koelling, J., Wallace, D. W. R., Send, U., & Karstensen, J. (2017). Intense oceanic uptake of oxygen during 2014–2015 winter convection in the Labrador Sea. *Geophysical Research Letters*, *44*(15), 7855–7864.

Körtzinger, A., Send, U., Wallace, D. W., Karstensen, J., & DeGrandpre, M. (2008). Seasonal cycle of O_2 and pCO_2 in the central Labrador Sea: Atmospheric, biological, and physical implications. *Global Biogeochemical Cycles*, *22*(1).

Li, H., Fedorov, A., & Liu, W. (2021). AMOC stability and diverging response to Arctic sea ice decline in two climate models. *Journal of Climate*, *34*(13), 5443–5460.

Lilly, J. M., & Rhines, P. B. (2002). Coherent eddies in the Labrador Sea observed from a mooring. *Journal of Physical Oceanography*, *32*(2), 585–598.

Lilly, J. M., Rhines, P. B., Schott, F., Lavender, K., Lazier, J., Send, U., & D'Asaro, E. (2003). Observations of the Labrador Sea eddy field. *Progress in Oceanography*, *59*(1), 75–176.

Lilly, J. M., Rhines, P. B., Visbeck, M., Davis, R., Lazier, J. R., Schott, F., & Farmer, D. (1999). Observing deep convection in the Labrador Sea during winter 1994/95. *Journal of Physical Oceanography*, *29*(8), 2065–2098.

Lozier, M., Li, F., Bacon, S., Bahr, F., Bower, A., Cunningham, S., ... others (2019). A sea change in our view of overturning in the subpolar North Atlantic. *Science*, *363*(6426), 516–521.

MacGilchrist, G. A., Johnson, H. L., Lique, C., & Marshall, D. P. (2021). Demons in the North Atlantic: Variability of deep ocean ventilation. *Geophysical Research Letters*, *48*(9), e2020GL092340.

McDougall, T. J., & Barker, P. M. (2011). Getting started with TEOS-10 and the Gibbs Seawater (GSW) oceanographic toolbox. *SCOR/IAPSO WG*, *127*, 1–28.

Mertens, C. (2000). *Open-ocean convection in the Labrador and Greenland Seas: plume scales and interannual variability* (Unpublished doctoral dissertation). ChristianAlbrechts University, Kiel.

Moore, G., Pickart, R. S., & Renfrew, I. A. (2008). Buoy observations from the windiest location in the world ocean, Cape Farewell, Greenland. *Geophysical Research Letters*, *35*(18).

Moore, G., Pickart, R. S., Renfrew, I. A., & Våge, K. (2014). What causes the location of the air-sea turbulent heat flux maximum over the Labrador Sea? *Geophysical Research Letters*, *41*(10), 3628–3635.

Morison, J., Andersen, R., Larson, N., D'Asaro, E., & Boyd, T. (1994). The correction for thermal-lag effects in Sea-Bird CTD data. *Journal of atmospheric and oceanic technology*, *11*(4), 1151–1164.

Renfrew, I. A., & Moore, G. (1999). An extreme cold-air outbreak over the Labrador Sea: Roll vortices and air–sea interaction. *Monthly Weather Review*, *127*(10), 2379–2394.

Rhein, M., Kieke, D., & Steinfeldt, R. (2007). Ventilation of the Upper Labrador Sea Water, 2003–2005. *Geophysical research letters*, *34*(6).

Rieck, J. K., Böning, C. W., & Getzlaff, K. (2019). The nature of eddy kinetic energy in the Labrador Sea: Different types of mesoscale eddies, their temporal variability, and impact on deep convection. *Journal of Physical Oceanography*, *49*(8), 2075–2094.

Roemmich, D., & Gilson, J. (2009). The 2004–2008 mean and annual cycle of temperature, salinity, and steric height in the global ocean from the Argo Program. *Progress in Oceanography*, *82*(2), 81–100.

Rudnick, D. L. (2016). Ocean research enabled by underwater gliders. *Annual Review of Marine Science*, *8*, 519–541.

Sathiyamoorthy, S., & Moore, G. W. K. (2002). Buoyancy flux at ocean weather station Bravo. *Journal of Physical Oceanography*, *32*(2), 458–474.

Straneo, F. (2006). Heat and freshwater transport through the central Labrador Sea. *Journal of Physical Oceanography*, *36*(4), 606–628.

Tagklis, F., Bracco, A., Ito, T., & Castelao, R. (2020). Submesoscale modulation of deep water formation in the Labrador Sea. *Scientific reports*, *10*(1), 1–13.

Troupin, C., Beltran, J. P., Heslop, E., Torner, M., Garau, B., Allen, J., ... Tintoré, J. (2015). A toolbox for glider data processing and management. *Methods in Oceanography*, *13*, 13–23.

von Oppeln–Bronikowski, N., de Young, B., Atamanchuk, D., & Wallace, D. W. (2021). Glider-based observations of CO_2 in the Labrador Sea. *Ocean Science*, *17*(1), 1–16. doi: 10.5194/os-17-1-2021

von Oppeln-Bronikowski, N., de Young, B., Bachmayer, R., Palter, J., Claus, B., Zhou, M., ... Foley, J. (2021). *Memorial University Ocean Glider Deployments: 2005–Present* [Dataset]. Retrieved from `https://www.seanoe.org/data/00681/79349/` doi: 10.17882/79349

Wong, A., Keeley, R., Carval, T., & the Argo Data Management Team. (2020). Argo quality control manual for CTD and trajectory data [Computer software manual]. Ifremer. doi: http://dx.doi.org/10.13155/33951

Woo, M. L. (2019). Ocean Glider delayed mode QA/QC best practice manual, Version 2.1. [Computer software manual]. Hobart, Australia: Integrated Marine Observing System. doi: 10.26198/5c997b5fdc9bd

Yashayaev, I. (2007). Hydrographic changes in the Labrador Sea, 1960–2005. *Progress in Oceanography*, *73*(3-4), 242–276.

Yashayaev, I., & Loder, J. W. (2016). Recurrent replenishment of Labrador Sea Water and associated decadal-scale variability. *Journal of Geophysical Research: Oceans*, *121*(11), 8095–8114.

Yashayaev, I., & Loder, J. W. (2017). Further intensification of deep convection in the Labrador Sea in 2016. *Geophysical Research Letters*, *44*(3), 1429–1438.

Yeager, S., Castruccio, F., Chang, P., Danabasoglu, G., Maroon, E., Small, J., ... Zhang, S. (2021). An outsized role for the Labrador Sea in the multidecadal variability of the Atlantic overturning circulation. *Science Advances*, *7*(41), 1–14. doi: 10.1126/sciadv.abh3592

Zhang, J., Weijer, W., Steele, M., Cheng, W., Verma, T., & Veneziani, M. (2021). Labrador Sea freshening linked to Beaufort Gyre freshwater release. *Nature communications*, *12*(1), 1–8.

Figure 1.

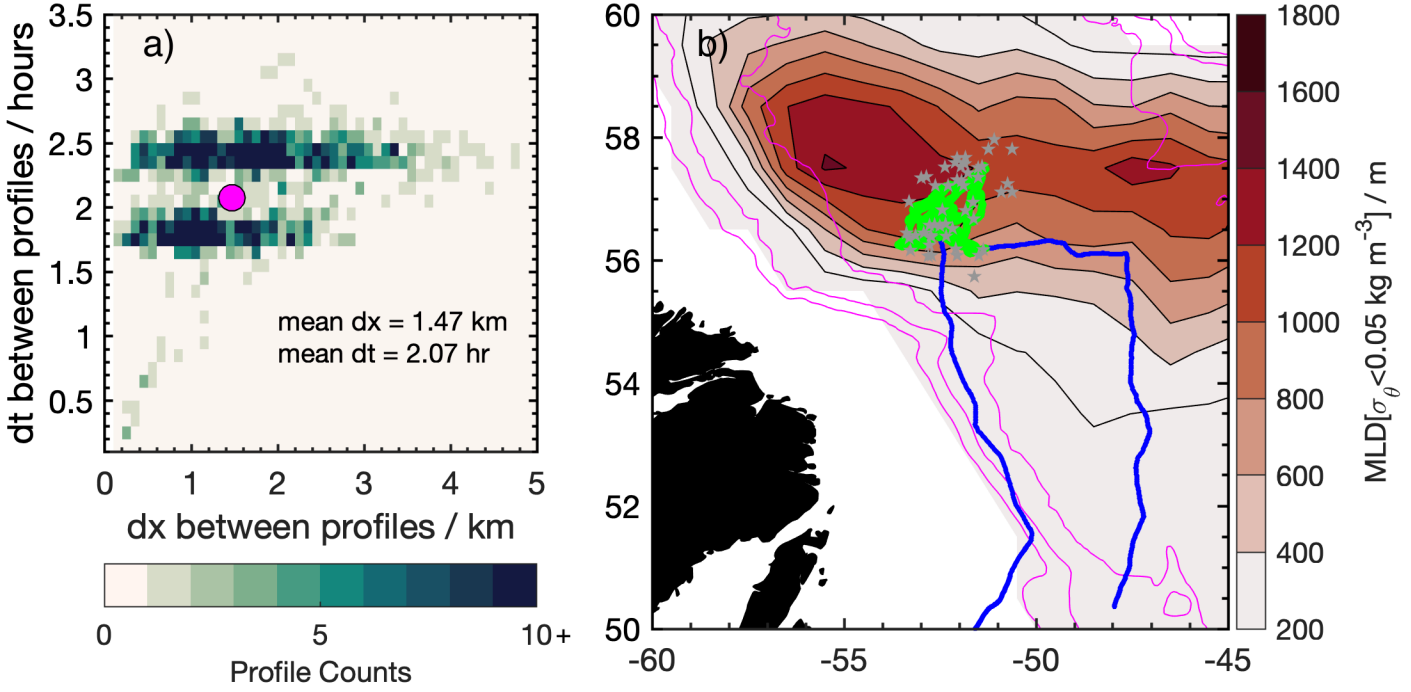
a)
dt between profiles / hours
dx between profiles / km
mean dx = 1.47 km
mean dt = 2.07 hr
0
5
10+
Profile Counts
b)
MLD[σ_θ<0.05 kg m^{-3}] / m
1800
1600
1400
1200
1000
800
600
400
200

Figure 2.

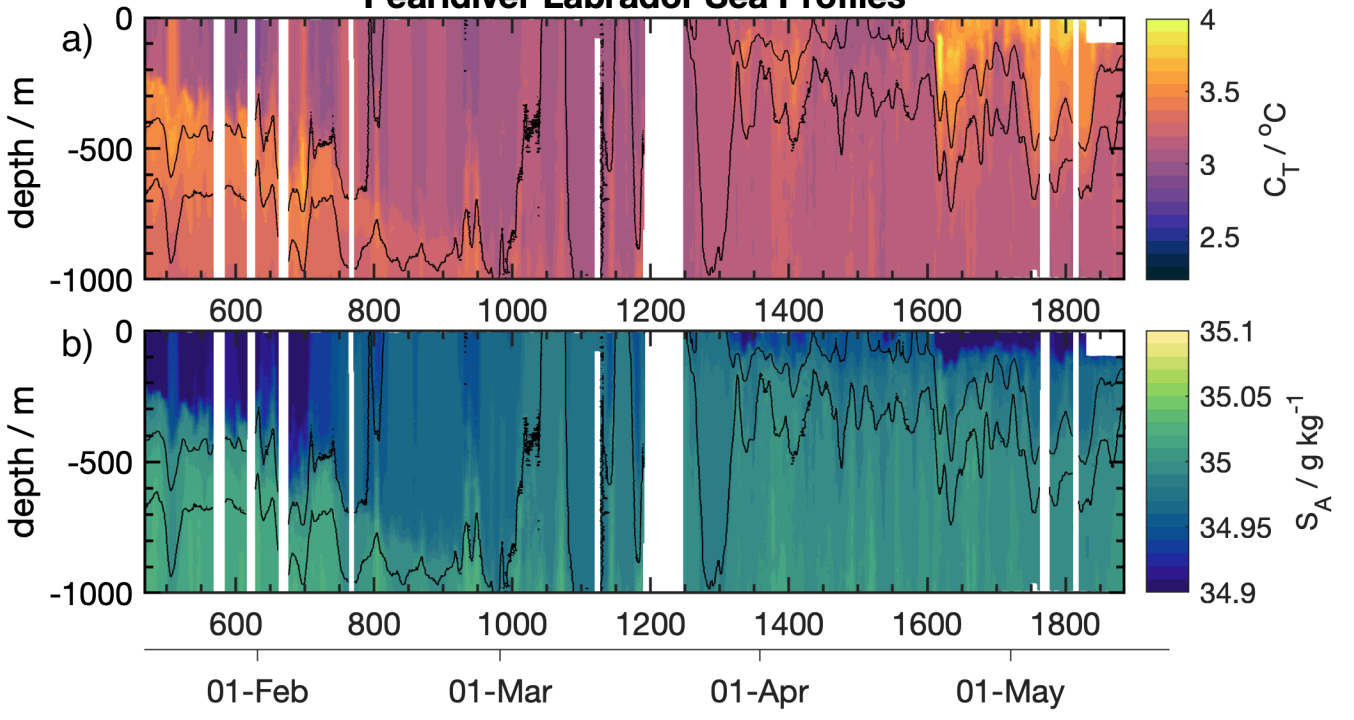
Pearldiver Labrador Sea Profiles
a)
b)
depth / m
0
-500
-1000
600
800
1000
1200
1400
1600
1800
4
3.5
3
2.5
C_T / °C
35.1
35.05
35
34.95
34.9
S_A / g kg^{-1}
01-Feb
01-Mar
01-Apr
01-May

Figure 3.

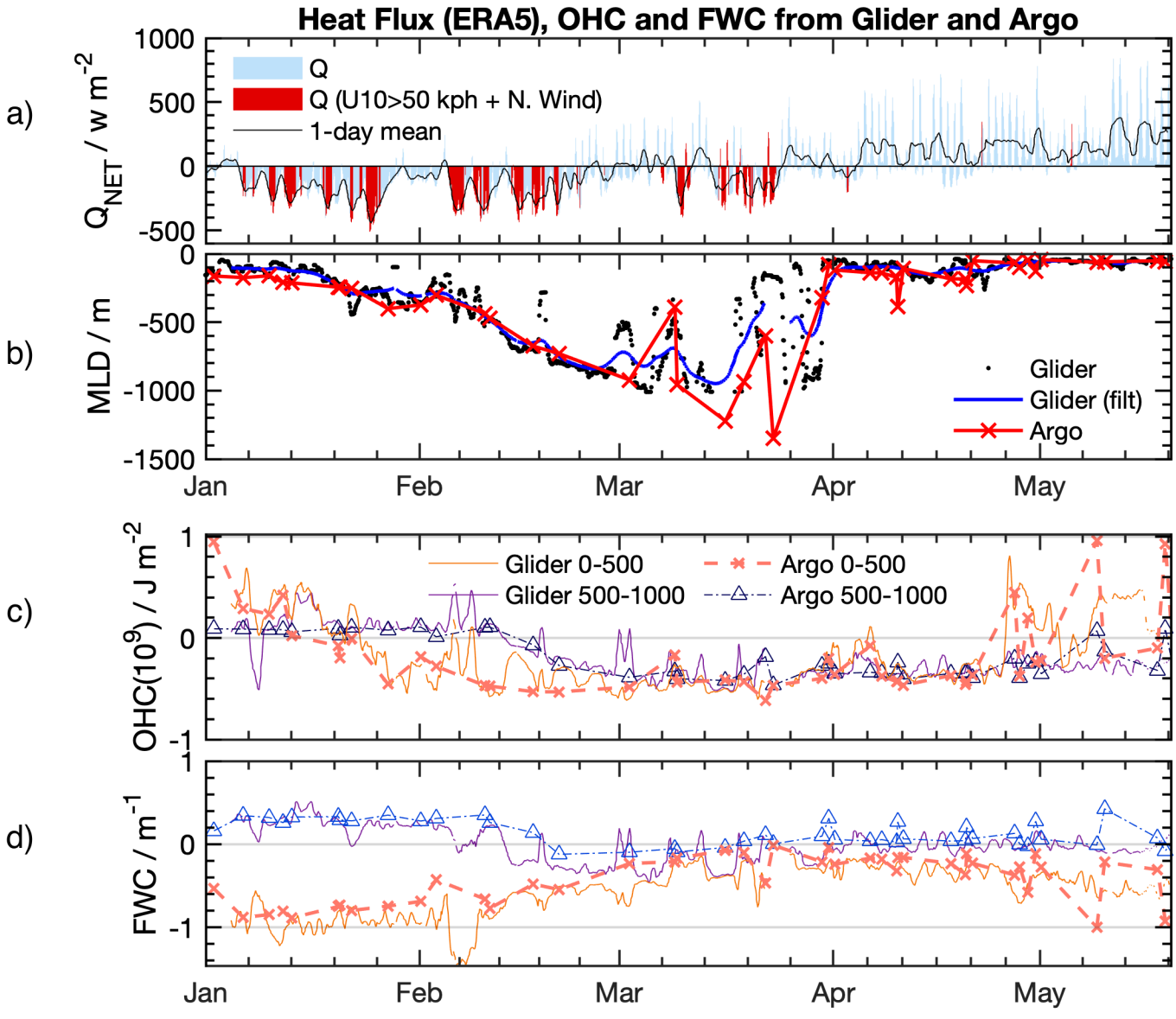
Heat Flux (ERA5), OHC and FWC from Glider and Argo
a)
b)
c)
d)
Q
Q (U10>50 kph + N. Wind)
1-day mean
Q_{NET} / w m^{-2}
MLD / m
Glider
Glider (filt)
Argo
OHC(10^9) / J m^{-2}
Glider 0-500
Glider 500-1000
Argo 0-500
Argo 500-1000
FWC / m^{-1}
Jan
Feb
Mar
Apr
May

Figure 4.

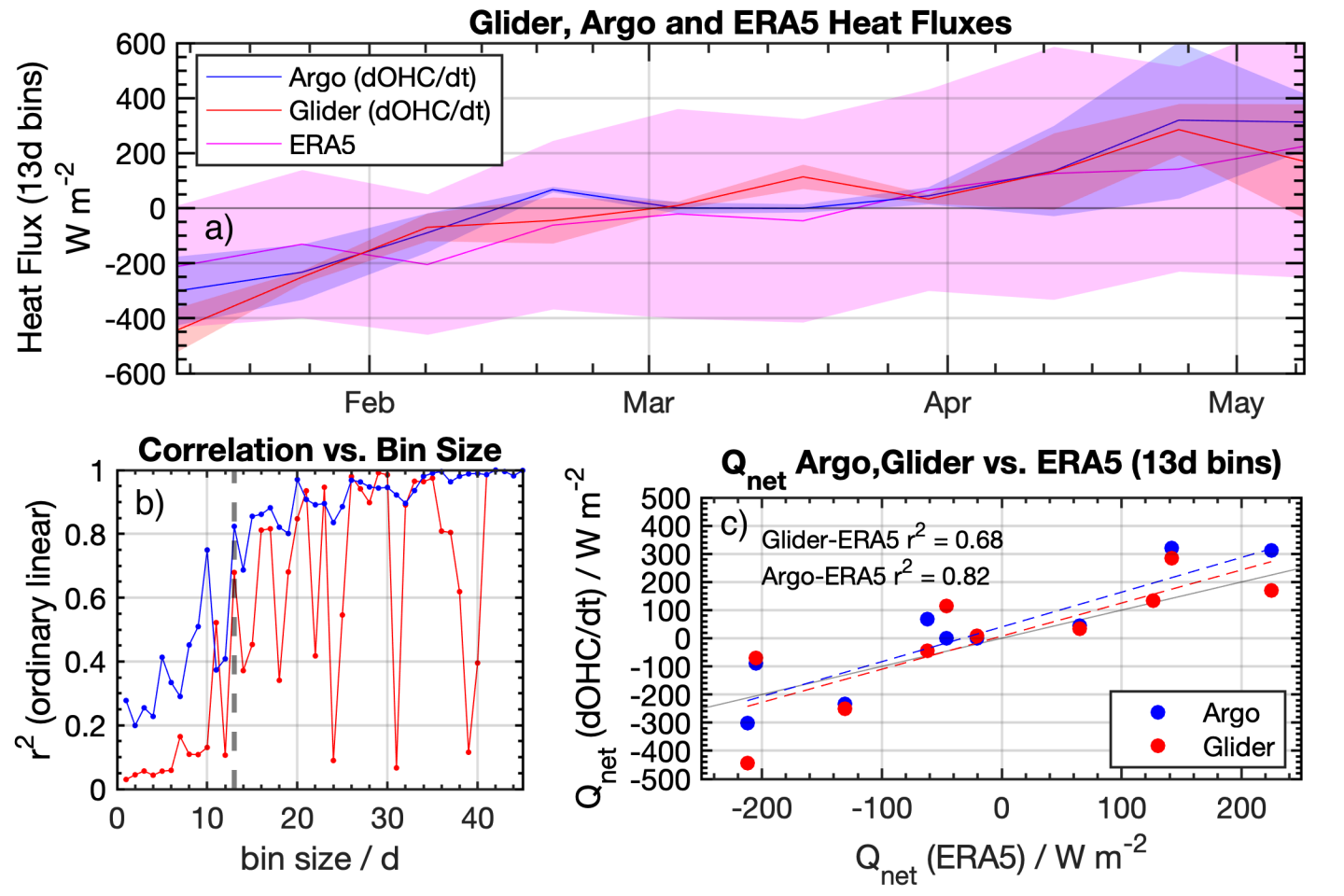
Glider, Argo and ERA5 Heat Fluxes
Argo (dOHC/dt)
Glider (dOHC/dt)
ERA5
a)
Heat Flux (13d bins)
W m-2
600
400
200
0
-200
-400
-600
Feb
Mar
Apr
May
Correlation vs. Bin Size
b)
r2 (ordinary linear)
bin size / d
Qnet Argo,Glider vs. ERA5 (13d bins)
c)
Glider-ERA5 r2 = 0.68
Argo-ERA5 r2 = 0.82
Argo
Glider
Qnet (dOHC/dt) / W m-2
Qnet (ERA5) / W m-2

Figure 5.

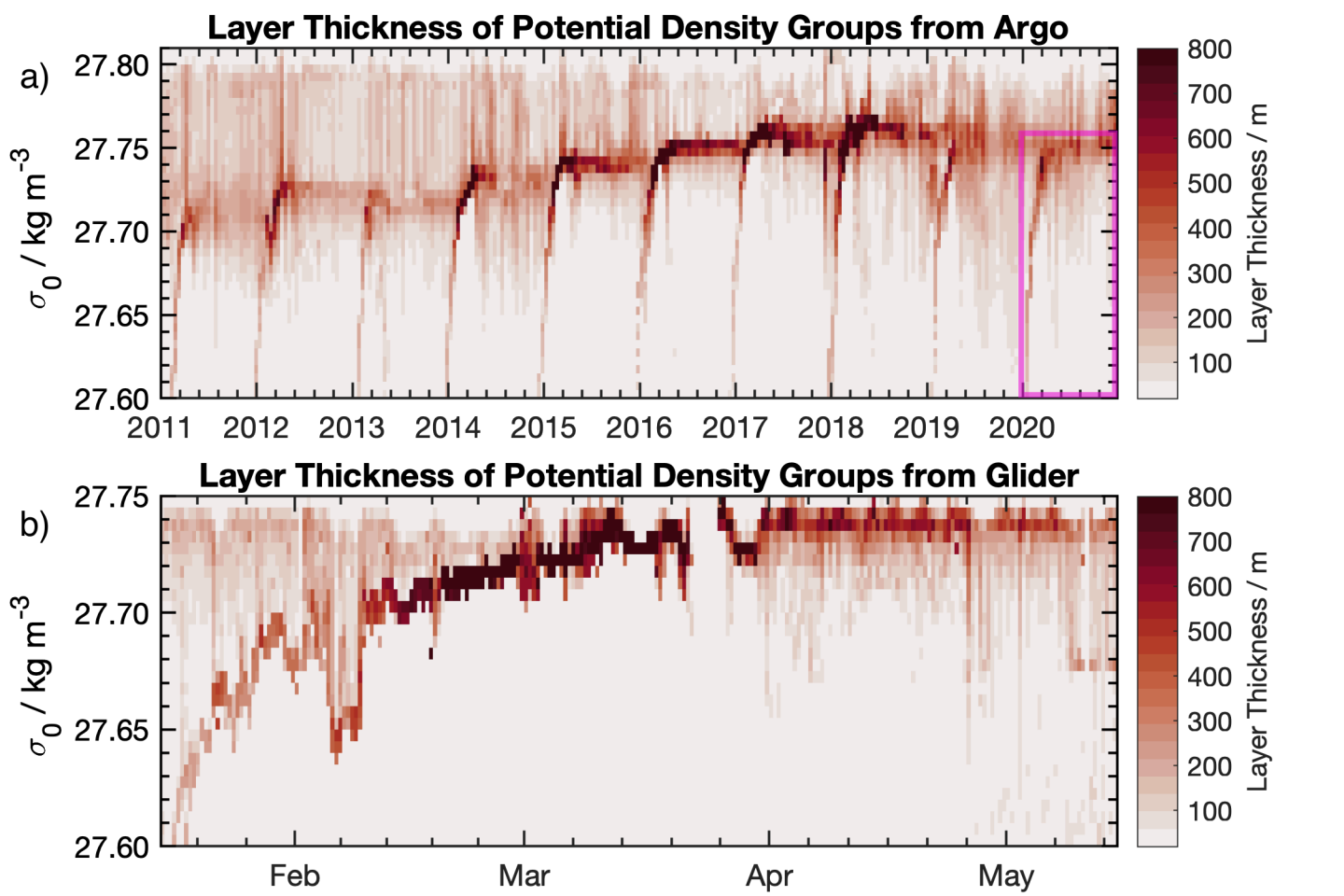
Layer Thickness of Potential Density Groups from Argo
a)
σ_0 / kg m^{-3}
27.80
27.75
27.70
27.65
27.60
2011
2012
2013
2014
2015
2016
2017
2018
2019
2020
800
700
600
500
400
300
200
100
Layer Thickness / m
Layer Thickness of Potential Density Groups from Glider
b)
σ_0 / kg m^{-3}
27.75
27.70
27.65
27.60
Feb
Mar
Apr
May
800
700
600
500
400
300
200
100
Layer Thickness / m

Figure 6.

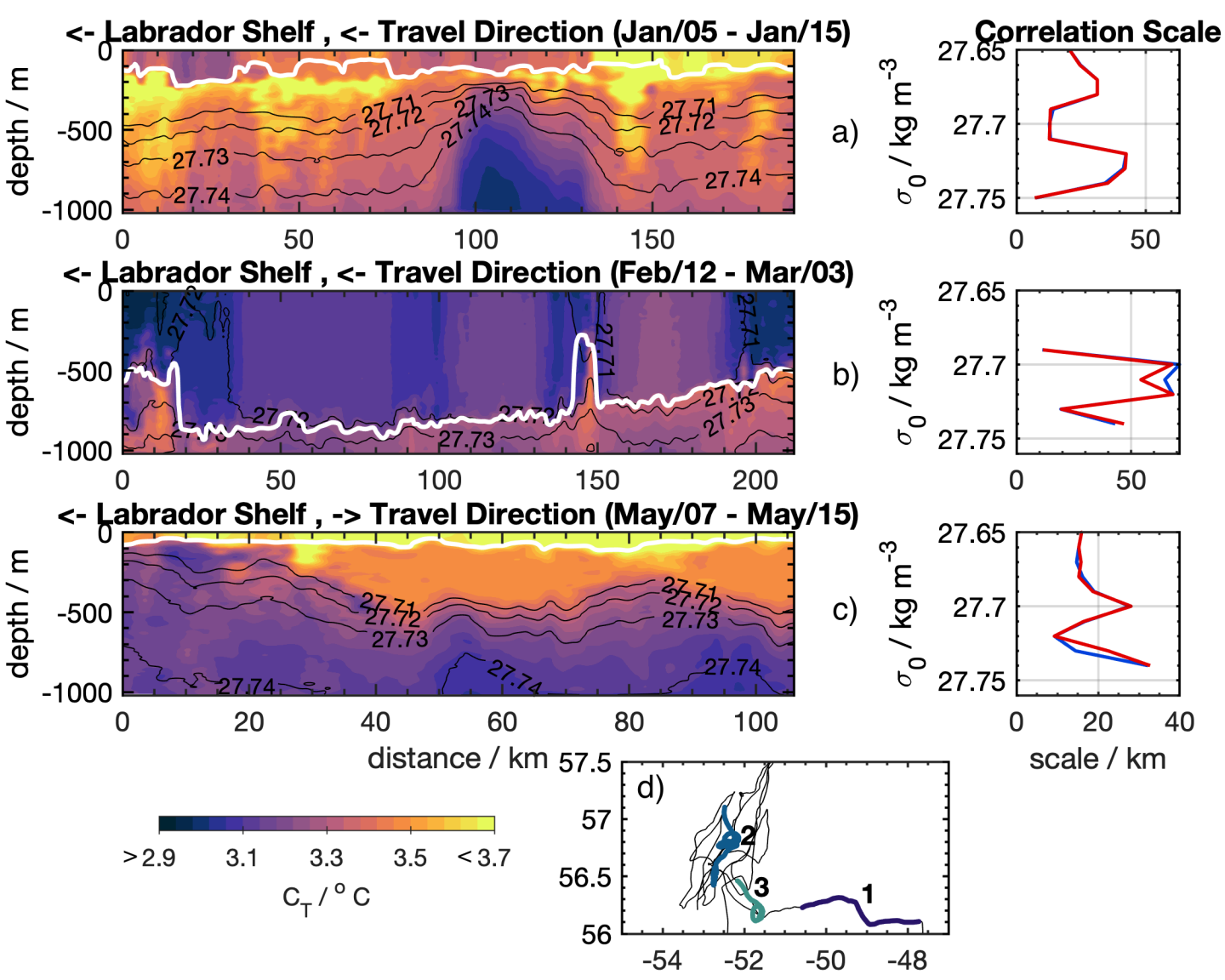
<- Labrador Shelf , <- Travel Direction (Jan/05 - Jan/15)
<- Labrador Shelf , <- Travel Direction (Feb/12 - Mar/03)
<- Labrador Shelf , -> Travel Direction (May/07 - May/15)
Correlation Scale
depth / m
distance / km
scale / km
σ_0 / kg m^{-3}
a)
b)
c)
d)
27.71
27.72
27.73
27.74
27.75
C_T / ° C
> 2.9
3.1
3.3
3.5
< 3.7
1
2
3

Figure 7.

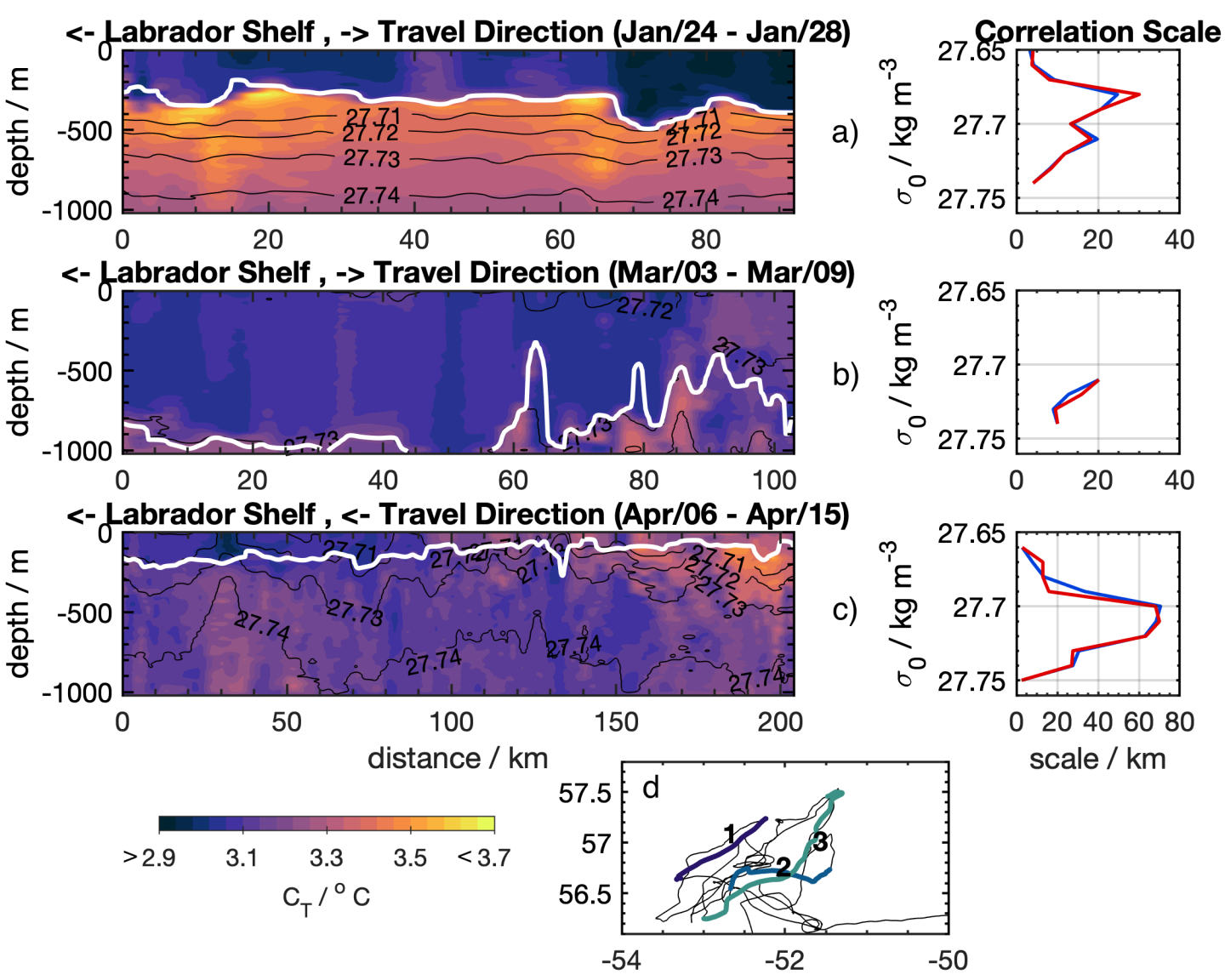
<- Labrador Shelf , -> Travel Direction (Jan/24 - Jan/28)
<- Labrador Shelf , -> Travel Direction (Mar/03 - Mar/09)
<- Labrador Shelf , <- Travel Direction (Apr/06 - Apr/15)
depth / m
distance / km
Correlation Scale
scale / km
σ_0 / kg m^{-3}
a)
b)
c)
d
C_T / ° C
> 2.9
3.1
3.3
3.5
< 3.7

Figure 8.

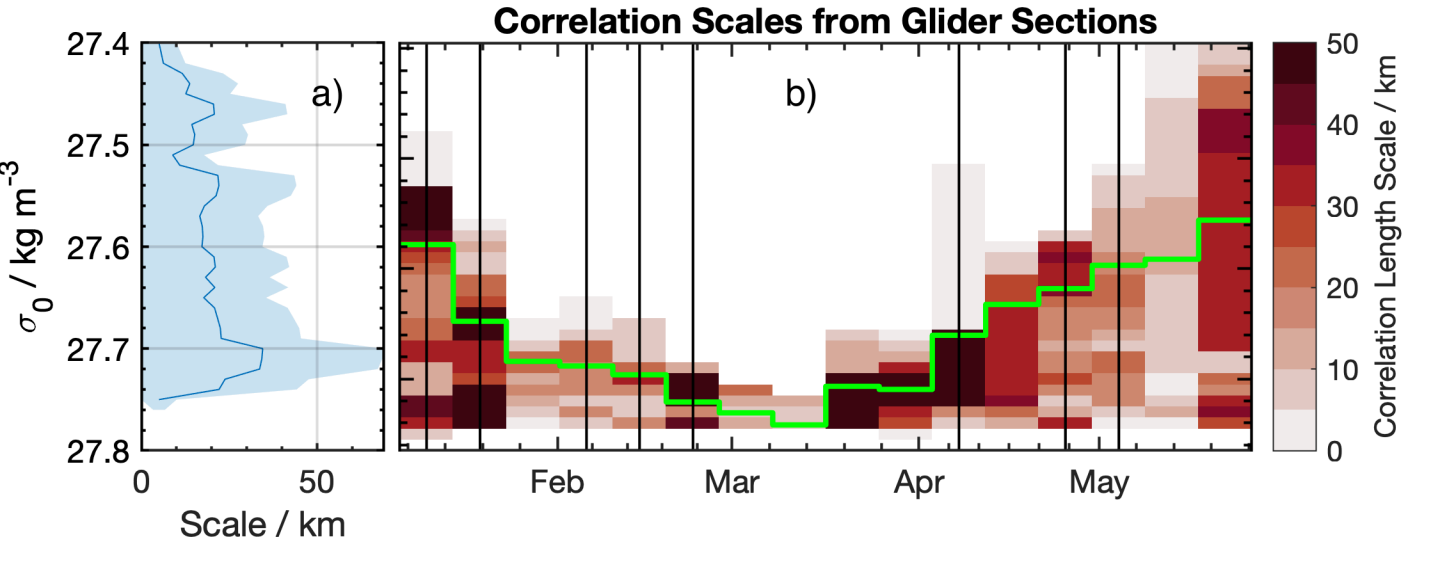
Correlation Scales from Glider Sections
a)
b)
27.4
27.5
27.6
27.7
27.8
σ_0 / kg m^{-3}
0
50
Scale / km
Feb
Mar
Apr
May
50
40
30
20
10
0
Correlation Length Scale / km

Figure 9.

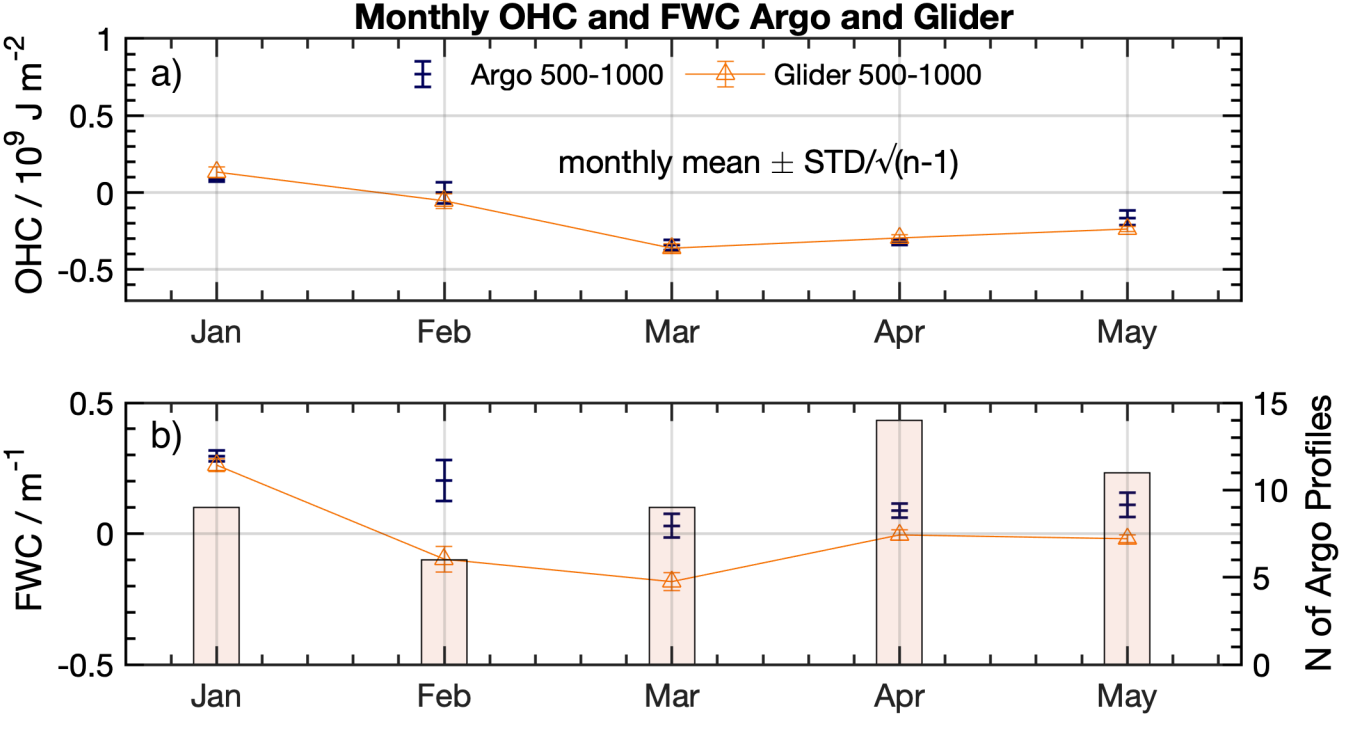
Monthly OHC and FWC Argo and Glider
a)
Argo 500-1000
Glider 500-1000
monthly mean ± STD/√(n-1)
OHC / 10^9 J m^-2
1
0.5
0
-0.5
Jan
Feb
Mar
Apr
May
b)
FWC / m^-1
0.5
0
-0.5
N of Argo Profiles
15
10
5
0
Jan
Feb
Mar
Apr
May

Figure 10.

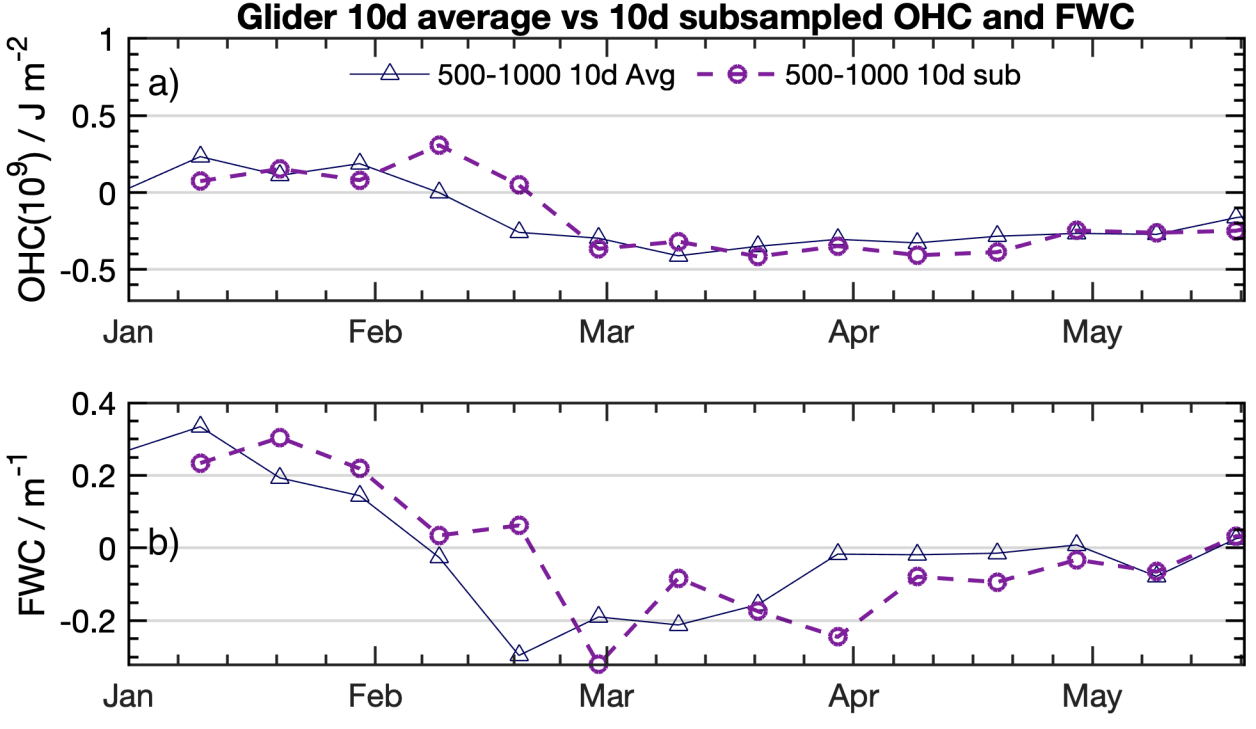
Glider 10d average vs 10d subsampled OHC and FWC
a)
500-1000 10d Avg
500-1000 10d sub
OHC(10^9) / J m^-2
1
0.5
0
-0.5
Jan
Feb
Mar
Apr
May
b)
FWC / m^-1
0.4
0.2
0
-0.2
Jan
Feb
Mar
Apr
May

Figure 11.

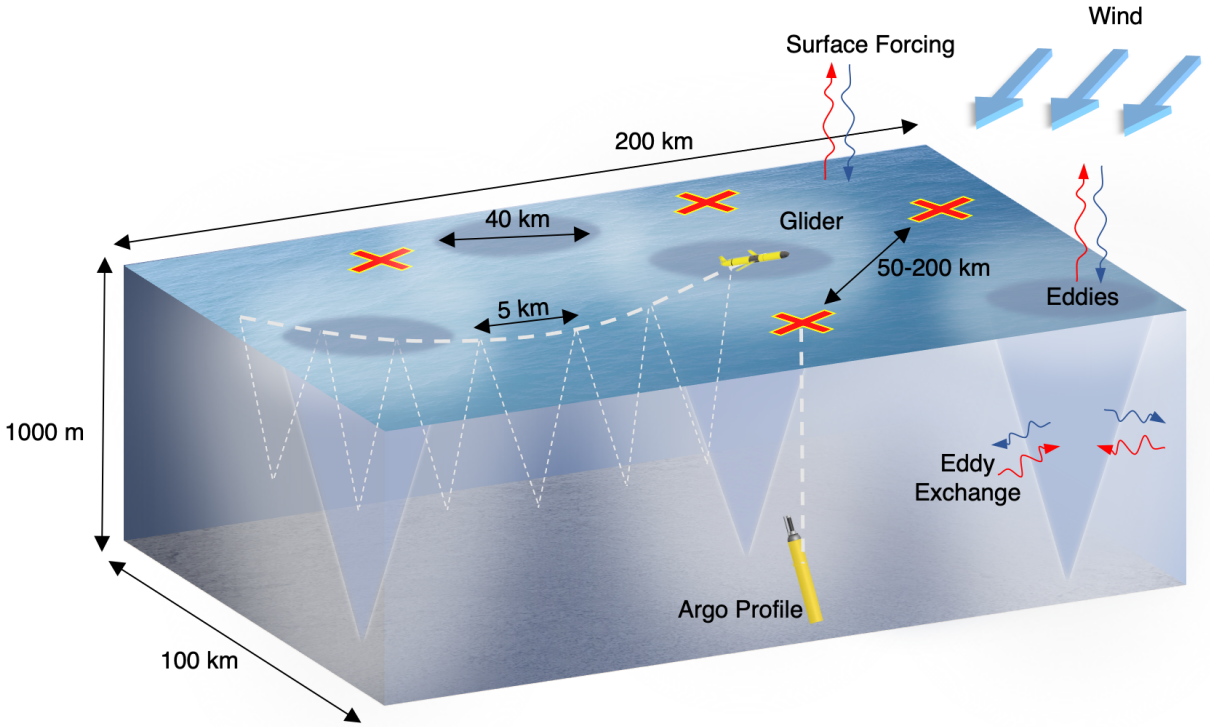
Wind
Surface Forcing
200 km
40 km
Glider
50-200 km
Eddies
5 km
1000 m
Eddy
Exchange
Argo Profile
100 km